energies

MDPI

Article

A New Technique for Estimating Stress from Fracture Injection Tests Using Continuous Wavelet Transform †

Mohamed Adel Gabry *, Ibrahim Eltaleb, Mohamed Y. Soliman and Syed M. Farouq-Ali

Department of Petroleum Engineering, The University of Houston, Houston, TX 77023, USA
* Correspondence: magabry@cougarnet.uh.edu
† Society of Petroleum Engineers Technical Conference and Exhibition, Houston, TX, USA, 3–5 October 2022.

Abstract: The diagnostic fracture injection test (DFIT) is widely used to obtain the fracture closure pressure, reservoir permeability, and reservoir pressure. Conventional methods for analyzing DFIT are based on the assumption that a vertical well is drilled in ultra-low permeability reservoirs with potential multiple closures but fails to consider horizontal wells. There is still significant debate about the rigorousness and validity of these techniques due to the complexity of the hydraulic fracture opening and closure process and assumptions of conventional fracture detection methods. The paper introduces a new method for detecting fracture closure pressure using the continuous wavelet transform (CWT). The new method aims to decompose the pressure fall-off signal into multiple levels with different frequencies using the CWT. This "short wavy" function is stretched or compressed and placed at many positions along the signal to be analyzed. The wavelet then convoluted the signal yielding a wavelet coefficient value. The signal energy is observed during the fracture closure process (pressure fall-off) and the fracture closure event is identified when the signal energy stabilizes to a minimum level. A predefined simple commercial fracture simulation case with known fracture closure, flow regime modeling, and actual field cases was used to validate the new methodology.

Keywords: continuous wavelet transform; diagnostic fracture injection test; hydraulic fracture; minimum horizontal stress; geothermal reservoirs

check for updates

Citation: Gabry, M.A.; Eltaleb, I.; Soliman, M.Y.; Farouq-Ali, S.M. A New Technique for Estimating Stress from Fracture Injection Tests Using Continuous Wavelet Transform. *Energies* **2023**, *16*, 764. https://doi.org/10.3390/en16020764

Academic Editor: Maria Grazia De Giorgi

Received: 2 December 2022
Revised: 23 December 2022
Accepted: 27 December 2022
Published: 9 January 2023

Copyright: © 2023 by the authors. Licensee MDPI, Basel, Switzerland. This article is an open access article distributed under the terms and conditions of the Creative Commons Attribution (CC BY) license (https://creativecommons.org/licenses/by/4.0/).

1. Introduction

1.1. Scope of Study

Estimating the minimum horizontal stress is a critical part of building formation geomechanical models, designing hydraulic fractures, designing drilling schedules, etc. Hydraulic fracturing design and execution need to calibrate the mechanical Earth model with a reliable method. This is performed to identify the formation stresses. Classical methods for obtaining the minimum horizontal stress of the formation relies on the open-hole well logs (Eaton (1969) [1]; Blanton and Olson (1999) [2]). These methods can be categorized into two main techniques. The first technique relies on compressional and shear sonic waves to estimate dynamic geo-mechanical properties. The second technique uses correlations to calculate the dynamic properties of the rock from conventional well-logging parameters, then calculates the minimum horizontal stress [3].

The actual in situ minimum principal stress of the formation is calculated by calibrating against the closure pressure from diagnostic pumping test [4]. That is performed by pumping a small volume of non-wall building fluids to create a small fracture and then analyze the pressure decline to know the pressure at which that fracture closes. That fracture closure pressure should be the average of the minimum principal stress for the area covered by the created fracture.

As no possible physical observation of the fracture propagation and closure in complicated subsurface formations, there are significant debates surrounding the various methodologies used to determine closure pressure. This is because of several reasons. The

first reason is that the hydraulic fracture propagation and closure process are fairly complicated due to the formation stress state, the presence of natural fractures, heterogeneity, and the anisotropy of the subsurface formations' properties. Conventional closure detection methods have pre-set assumptions to simplify the state of the subsurface formation. Some of them may simplify the leak off to carter leak off, whilst other methods assume the constant compliance or make certain assumptions regarding the flow regimes or the state of injection. Many tests may deviate from the assumed pre-set conditions. The detected closure be confused by the formation pressure response after the fracture closure. The pressure change propagates in the formation and produces behavior that may be confused with fracture closure detection.

Although fracture closure is defined as the pressure at which a fracture closes, there is an attempt to detect the contact pressure when the two fracture faces first come into contact with one another. Assuming that closure pressure does not really exist, there is an aperture between fracture faces. Complications regarding how the fracture propagates and closes cause the interpreted fracture closure pressure debatable. In most cases, the industry workers try various methods to determine the range of closure pressure. To date, there is no global technique that can detect closure without pre-assumptions. Each of the conventional methods detects the closure from a specific point of view with certain pre-assumptions. This paper introduces an innovative method to find the closure pressure using the wavelet transform technique as a general technique without any pre-assumptions. It uses an independent mathematical microscope to find the fracture closure pressure in the pressure fall-off signal. The new technique is validated using different ways: using simulated synthetic pressure data from a fracture simulator and using flow regime modeling by reverse calculating a pressure decay signal assumed to be both before fracture closure and after fracture closure flow regimes. The main advantage of this technique is that there is no need to know formation parameters in advance or have a pre-prescribed testing procedure.

Since the beginning of the 1990s, the science and engineering applications of wavelet transform have increased at a remarkable growth rate. Thousands of peer-reviewed journals are now interested in wavelet transform applications covering numerous disciplines such as fluids, medicine, and fractal geometry. However, its use in the oil and gas industry and geothermal energy has been limited to date. A lot of the data recorded in multiple disciplines are considered as signals to be analyzed to understand the physics-based models covering the many applications. For example, Germán-Salló et al. (2018) [5] introduced a method for crack detection in manufacturing systems using digital signal processing methods.

Signal processing is widely used in the medical field to detect heart problems by analyzing electrocardiography (ECG) signals. Research in the medical field deploys wavelet transform to compare the ECG signals of a healthy heart to another ECG signal associated with a diseased heart. The same methodology is adopted in the industrial application of signal processing to predict motor failure. For instance, the analysis of the vibration signal of a motor can help detect bearing failure when the recorded signal is compared to a functional motor.

With the ongoing digitalization of the modern oil and gas industry and geothermal energy industry, the same technique can be used in the analysis of hydraulic fracturing. In this case, changes in pressure and rate over time are recorded during the fracture propagation stages, proppant placement, and fracture closure to determine what is happening thousands of feet below the Earth's surface during hydraulic fracturing treatment. The most common methodology used by researchers for engineering wavelets applications is to try to find a correlation between the features detected from the signals and the actual physical response of the system. The main problem with this methodology in hydraulic fracturing is the complexity of hydraulic fracturing propagation and closure due to fracture face roughness or natural fracture intensity and directions and a lot of other factors. This may be complex not only because of the heterogeneity of the reservoir, but also because of the interaction of the hydraulic fracture with natural fractures, fissures, and other geologic

features. Thus, all the complicating factors should be removed from the system to find a signal representing a closure event in a homogeneous reservoir with no geologic complexities. In order to understand the CWT behavior during fracture closure, a numerical fracture simulator is used in this study.

The application of wavelet analysis in the oil industry was pioneered twenty years ago by Soliman et al. (2003) [6] as an application for well-test analysis and fracturing. The wavelet transform technique is a data transform technique that convolves the pressure and/or temperature data using a short wavy signal called "wavelet". This convolution can be performed at discrete points in the discrete wavelet transform (DWT) or continuously using the CWT. The wavelet transform provides a representation of the pressure signal by letting the translation and scales of the wavelets vary continuously. This enables the analyst to find the details of the pressure data by observing the wavelet energy spectrum for the monitored signal (pressure and/or temperature).

As the DWT is computationally cheaper, it was used as the first step to detect fracture closure. The main disadvantage of using the DWT is its requirement of a uniform sampling rate and the detected closure pressure changes with an increasing level of decomposition. Soliman, Unal, Siddiqui, Rezaei, and Eltaleb (2019) [7,8] initiated a methodology to detect the fracture closure pressure using the DWT. Determining the closure pressure in this methodology is based on analyzing the detail levels to pick the time when the variance changes. Eltaleb et al. (2020) [9] and Eltaleb et al. (2021) [10] improved the rigor of the technique using an energy density plot. The technique was compared to the G-function technique and showed good agreement. The DWT technique involves a multiresolution wavelet decomposition that breaks the (recorder pressure) signal into high pass (noise) and low pass (approximation) components at various levels. The plot of energy distribution in time is constructed using the energy of the high pass component (noise) at different decomposition levels. These plots provide means of capturing the physical changes in the fracture system through pressure fall-off. They represented the noise energy in the recorded pressure at different frequency levels. The closure pressure in this methodology was determined based on changes in the noise energy of the recorded pressure and where it drops to a minimum stabilized level.

This paper introduces a closure detection technique similar to that introduced by Eltaleb et al. (2021) [10], however, using the CWT. Using the CWT does not need a uniform sampling rate and captures all signal details. CWT can be used as a method for detecting the fractal dimension which is one of the key features of complex wavelets that is sometimes referred to as a "mathematical microscope" to detect the features. Using CWT was recommended by Fatmir (2020) through personal communication. CWT can be used as a filter to detect the signal features. It has the flexibility to be used with or without a uniform sampling rate. Thus, it could be validated using any type of data. This new method was applied to both the fracture simulator data and actual field data. The synthetic data were produced using a commercially available fracture simulator developed by Barree (1983) [11] based on fracture propagation and closure simulation principles with predefined fracture closure. Azlinda et al. (2010) [12] showed good agreement between the used fracture simulator with down-hole events in a stacked fluvial pay system. The CWT technique showed success with the actual real field data conducted on one of the oil and gas fields and in another case in a geothermal reservoir.

1.2. History of Closure Pressure Detection Techniques

The basic concept of classical methods of closure event detection from the pressure decay of the diagnostic fracture injection test is combining the basic concepts of well testing and hydraulic fracture analysis. After hydraulic fracturing was first introduced by Clark (1949) [13], it was recognized that hydraulic fracturing could be used as a method to estimate the magnitude of minimum principal stress (Hubbert and Willis (1957) [14]; Godbey and Hodges (1958) [15]; Kehle (1964) [16]; Haimson and Fairhurst (1967) [17]; Hickman and Zoback (1983) [18]). The main idea was to pump fluid at a pressure higher

than the fracturing pressure, to initiate a hydraulic fracture and propagate it through the formation. The minimum principal stress can be estimated from pressure measurements during and after injection. Nolte (1979) [19] extended the applicability of fracturing tests by developing analytical techniques that can be used to estimate fluid leak-off parameters. These techniques can be used to obtain the leak-off rate of complex fluids such as linear gel or cross-linked gel. These tests are typically called mini-frac tests (McLennan and Roegiers, (1982) [20]) or fracture calibration tests (Mayerhofer and Economides (1993) [21]). This is performed to estimate the efficiency of the fracturing fluid after the interpretation of the minimum horizontal stress. One of the most widely used functions to obtain the closure pressure is G-function (Nolte (1979) [19]). Several techniques have subsequently been published as essential parts of the analysis, including those by Castillo (1987) [22] as well as Barree and Mukherjee (1996) [23]. Further modifications for the analysis were added, for example, by Mayerhofer and Economides (1993) [21] and Mayerhofer et al. (1995) [24] showed how to remove the filter cake effect and its effect on the fluid leak-off factor from the analysis. The recent development of the shale gas reservoirs came out with a new test that uses the non-wall building fluid instead of the cross-linked gel or linear gel. It is called the "diagnostic fracture injection test" (DFIT). It is routinely performed in unconventional reservoirs due to the incapability to flow the well to do a pressure transient analysis. The DFIT is used to obtain the best estimates for stress, permeability, and pore pressure (Craig and Brown (1999) [25]. The analysis of pressure decay data has two parts.

The first part of the DFIT analysis is called "Pre-closure analysis methods" which are usually based on techniques from Nolte (1979) [19] and Mayerhofer and Economides (1993) [21], Mayerhofer et al. (1995) [24], Barree and Mukherjee (1996) [23], and Barree et al. (2009) [26]. These methods are used to estimate the closure pressure and calibrate the minimum principal stress. The second part is called 'Post-closure' analysis methods which are usually based on techniques from conventional well testing (Gu et al. (1993) [27]; Soliman et al. (2005) [28]; Craig and Blasingame (2006) [29]) or the 'linear flow time function' technique developed by Nolte et al. (1997) [30]. Due the development of unconventional reservoirs, multiple DFIT interpretation techniques have recently been developed by Marongiu-Porcu et al. (2011; 2014) [31,32], Soliman and Kabir (2012) [33], Soliman and Gamadi (2012) [33], Cramer and Nguyen (2013) [34], Padmakar (2013) [35], Wallace et al. (2014) [36], Meng et al. (2014) [37], Craig (2014) [38], Zanganeh et al. (2018) [39], and Hawkes et al. (2018) [40].

One of the noticeable techniques is the compliance method that was recently introduced by McClure et al. (2014; 2016) [41,42] and Jung et al. (2016) [43]. This technique usually leads to an earlier and higher stress estimate in contrast to the commonly used tangent method (Barree et al. (2009) [26]) which is considered a modifications to Nolte's (1979) [19] technique. The technique introduced a new concept which is contact pressure instead of closure pressure. McClure et al. (2016) [42] and Jung et al. (2016) [43] performed detailed DFIT simulations considering the effect of a residual aperture fracture after the contact between the fracture walls. Simulations indicate that, in low permeability formations, the contacting of the fracture walls causes the magnitude of the pressure derivative to increase, resulting in a pressure signal that was previously interpreted as the height recession or closure of transverse fractures (Barree et al. (2009) [26]. Wang and Sharma (2017) [44] reproduced these findings and proposed a modified approach for estimating stress called the 'variable compliance method'. Currently, there are two main closure detection techniques that are used by the industry, the tangent method, and the compliance method.

The initial technique of the G function introduced by Nolte (1979) [19] relied on several assumptions for the pumping and shut-in periods with some simplified concepts of how a fracture propagates and closes. Nolte (1979) [19] provided the G time function to detect the changes in the pressure during the shut-in period of the diagnostic pumping. The second derivative (GdP/dG) is used to detect the closure. The closure defined by this technique is the pressure at a time when the deviation from the straight line starting from

zero in GdP/dG occurs. The detailed equations for the G time function were discussed by Nolte (1979) [19]. Castillo (1987) [22] added the condition that dP/dG should be with zero slopes at the same point. The tangent method was introduced to cope with the complicated fracture closure as a modification for the Nolte (1979) [19] technique. The tangent method proposed four types of leak-off in the formation during the closure, normal leak-off, pressure-dependent leak-off, transverse storage leak-off or height recessions, and tip extension leak-off. It is taken from a plot of GdP/dG versus G. A straight line is drawn from the origin to the tangent to the curve. The closure pressure is defined as the pressure when the GdP/dG starts to deviate downward. The pressure at that point is taken as the tangent method stress estimate. The tangent method was developed to match numerical simulations by Barree and Mukherjee (1996) [23] and Barree et al. (2009) [26]. Their work introduced a G-function signature for each type of leak-off. Each type of leak-off can characterize specific reservoir properties such as the presence of natural fractures, the presence of lower permeability streaks or weak barriers surrounding the pay zone. The tangent method in many cases shows a monotonic increase which makes the closure pressure too low to be identified. The tangent method is affected by the formation response after the fracture closure. It is normally associated with the square root of time and log–log analysis, as recommended by Baree et al. (2009) [26]. The pre-closure flow regime and post-closure flow regimes should be identified to support the closure detected using the tangent method. The second derivative of pressure to the square root of time should show a local peak at the closure. The relations between the log–log, square root of time, and tangent method were discussed in detail by Baree et al. (2009) [26]. The log–log technique and square root of time method can be combined as the "Holistic Fracture Diagnostics" as described by Baree et al. (2007) [45].

The compliance method for estimating stress was developed from mathematical solutions of the fracture closure process (McClure et al. (2016) [42]). As per the compliance method, the very early part of the shut-in is ignored as the pressure drops very rapidly. This part of the transient is ignored because it is caused by the dissipation of near-wellbore tortuosity related to the initiation of a transverse hydraulic fracture from a horizontal well. The straight section of the pressure versus G-time plot can be extrapolated back to the y-intercept to estimate the pressure in the far-field fracture at shut-in (the so-called effective initial shut-in pressure). After the initial period, the pressure curve settles into an approximately straight line. The 'compliance method' of estimating stress identifies the contact pressure at the point where the derivative increased from the minimum and subtracts 75 psi to account for a stress shadow from the residual aperture (McClure et al. (2019) [46]). The 75 psi adjustment is based on a numerical simulation that matches the field DFITs (McClure et al. (2019) [46]).

When the fracture walls contact, the stiffness increases, and the storage coefficient drops as per Sneddon (1946) [47]. This causes the dP/dG to increase when the fracture walls come into contact. McClure et al. (2016 [42], 2019 [46]) note that, because of the roughness of the fracture walls, the fluid pressure may be higher than the minimum principal stress when the walls come into contact. Thus, it is recommended to estimate the closure pressure as 75 psi lower than the contact pressure based on numerical simulations. The contact pressure is estimated by plotting the magnitude of dP/dG and identifying the point where this derivative reaches a minimum and begins to increase. This is the so-called 'compliance' method stress estimate. It is noticeable that the 'compliance method' is close to the classical method by Nolte (1979) [19]. However, an upward deflection in dP/dG is not always seen in the shut-in transients.

In a lot of cases, dP/dG continuously decreases during the shut-in. McClure et al. (2019) [46] discussed the possible causes of the lack of an upward deflection. That may be due to the excessive near-wellbore tortuosity as the fracture closes almost immediately after shut-in. The monotonic dP/dG might arise from the continued fracture propagation after shut-in. One of the key assumptions of G-function is that the fracture does not propagate after shut-in. This makes the G-function not accurate in many cases. McClure

et al. (2019) [46] recommended interpreting tests with a monotonic dP/dG as indicating 'rapid closure' in vertical wells where the near wellbore tortuosity is usually minimal and supplementing dP/dG plots with plots of 'relative stiffness' versus pressure. The relative stiffness is not a normalized value calculated to be proportional to the system stiffness. In tests where near-wellbore tortuosity is possible, McClure et al. (2019 [46]; 2022 [48]) recommended declining to provide a stress estimate and labeling the stress uninterpretable. McClure et al. (2022) [48] found that fifty-nine percent of cases showed a clear upward deflection; twenty-five percent of cases showed an adequate upward deflection; and sixteen percent of cases showed no indication of an upward deflection (i.e., a monotonic decrease in dP/dG).

From the previous discussions, closure detection is still open for research and needs more studies to understand the complications of fracture closure without pre-assumptions and fewer data requirements, which is the main advantage of wavelet transform techniques.

2. Methodology

2.1. Wavelet Transform

Wavelet transform is a mathematical transformation applied to signals to obtain information that is not readily available. This signal can be pressure or any parameter recorded during field operations. In practice, most signals are in the time domain in their raw format and plotted as a time–amplitude representation of the signal. As a result, this is not always the best representation of the signal for most signal processing-related applications; hence, the most valuable features are usually hidden in the signal frequency.

Several transformations may be used to analyze the acquired signals. Fourier transforms (FTs) are the most widely used signal processing technique that gives signal frequency information. However, it does not provide timely information on which those frequency components exist. FT works best in the analysis of stationary signals whose time domain is periodic; then, the time domain signal can be converted into a combination of sine and cosine waves to infinity duration (Rioul and Vetidsaerli (1991) [49]).

One modification for the Fourier transform is the windowed Fourier transform (WFT). It is a tool for extracting local-frequency information from the non-stationary signal. The signal is divided into small stationary segments through window functions whose width must equal the part of the signal where it is stationary. As discussed by Kaiser (1994) [50], WFT is prone to inaccurate results due to the aliasing of high- and low-frequency components that do not fall within the window function proposed by the technique. Wavelet transform (WT) has a dynamical frequency spectrum and can represent the signals in both the time and frequency domains. Figure 1 summarizes the difference between each signal representation. As the wavelets analysis has a high dynamical frequency and a high resolution in both frequency and time domains, it is preferred for signals with a wide range of dominant frequencies and time–frequency localization independence.

Wavelet transform analysis uses small wavelike functions known as wavelets. Mathematically, it can be defined as the convolution of the signal with the wavelet function. Figure 2 shows a few of the most common wavelet types.

Wavelets can be manipulated through translation (i.e., moving the wavelets along the time axis) and scale (i.e., stretching and squeezing the wavelet at a particular point in time). The scale and translation of wavelets govern parameters (b) and (a), respectively, in Equation (1).

$$T(a,b) = \frac{1}{\sqrt{a}} \int_{-\infty}^{\infty} x(t) \psi^* \left(\frac{t-b}{a} \right) dt \quad (1)$$

The Equation (1) comprised both the signal $x(t)$, which could represent the pressure, temperature, or any time series data, as well as the $(\psi^*(t-b)/a)$ mother wavelet function. The wavelet transform works by superimposing the wavelet function on an arbitrary signal, as illustrated in Figure 3. Time segments A and B, where both the wavelet and original signal agree (positive or negative), will result in a large positive transformation value of

the integral given by Equation (1). On the contrary, in regions C, D, and E, when the wavelet and the signal have opposite signs, the overall transformation results in a negative contribution to $T(a, b)$.

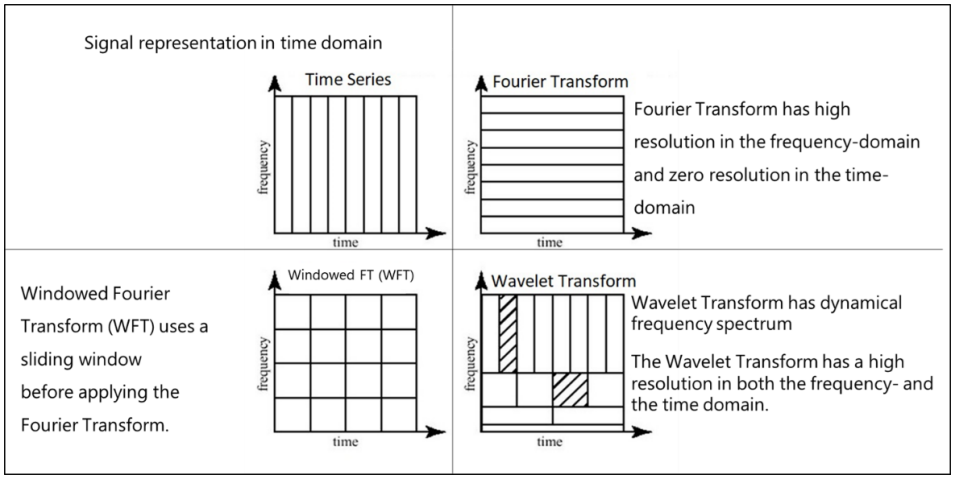


Figure 1. Comparison between different signal representations.

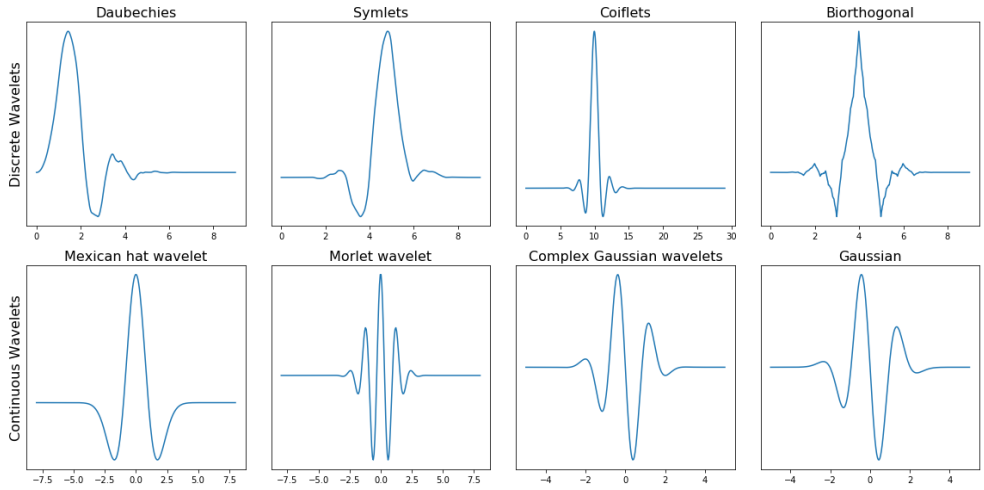


Figure 2. Shapes of different wavelet transform families.

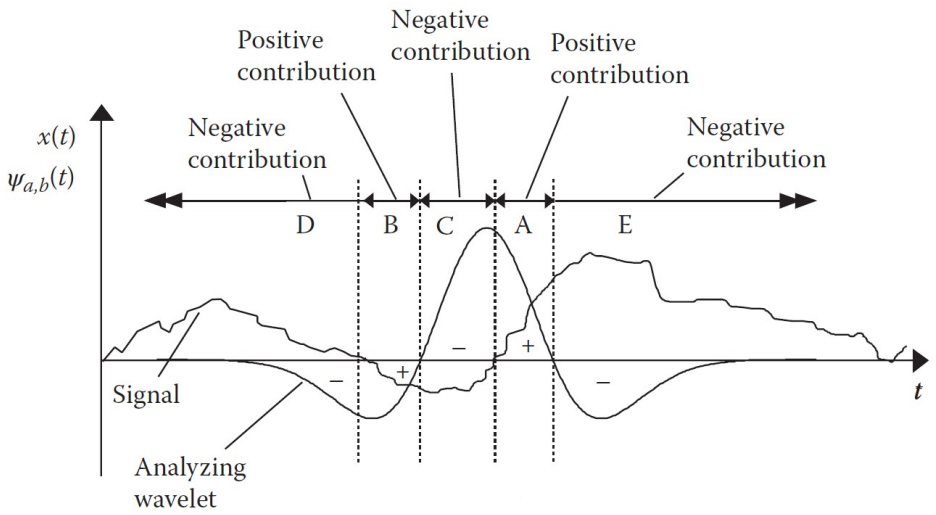


Figure 3. Mechanism of wavelet transform [51].

When using complex wavelets, the resulting coefficient consists of both real and imaginary parts. Fourier transforms of complex wavelets are zero for negative frequencies. Therefore, we can separate the phase and frequency components within the signal using complex wavelets. For instance, taking Fourier to transform the Mexican hat wavelet and then performing an inverse Fourier transform after neglecting the zero components in the Fourier transform will create a complex wavelet. It produces a less oscillatory transform than in the case of real wavelets because a complex wavelet only responds to the non-negative frequencies of the particular real signal. Therefore, it outperforms real wavelets in detecting and tracking instantaneous frequencies (Guerrero, A.P., and Paredes, G. E. (2018) [52]). Complex wavelet transform is used in our analysis, which is defined by Equation (2) where the first part is the normalization factor, the second part is the complex sinusoid, and the final part is the Gaussian bell curve.

$$\psi(t) = \frac{1}{\pi^{1/4}} e^{i2\pi f_0 t} e^{-t^2/2} \tag{2}$$

To inspect the multi-scale dimensional characteristics of a signal using complex wavelets, the Wavelet Transform Modulus (WTM) can be calculated using Equation (3).

$$T(a,b) = \sqrt{[Re(T(a,b))] + [Im(T(a,b))]} \tag{3}$$

One of the main features of the signals that can be observed and analyzed to identify the system properties is the analysis of signal energy. For any signal, the total energy contained in a signal, $x(t)$, is defined as its integrated squared magnitude as in Equation (4) with the condition that the signal must contain finite energy.

$$E = \int_{-\infty}^{\infty} |x(t)|^2 dt \tag{4}$$

The relative contribution of the signal energy contained at a specific scale (a) and location (b) is given by the two-dimensional wavelet energy density function:

$$E(a,b) = |T(a,b)|^2 \tag{5}$$

The plot $E(a)$ versus time (different location parameters b values) at different dilation parameter values (scale) (a) can be plotted in a plot called a scalogram. From the scalogram, the location and scale of dominant energetic features within the signal can be detected from the scale-dependent wavelet energy spectrum of signal $E(a)$ at a specific scale. A plot of $E(a,b)$ as a function of time and frequency is known as a scalogram. Scalograms are usually plotted with a logarithm and a scale axis. For example, Figure 4 shows a scalogram for The Nino3 SST monthly climate time data series analyzed using Morlet wavelets (Torrence and Compo (1998) [53]), as discussed by Addison, P.S. (2016) [51].

The features that are detected at small scales, the compressed wavelet, are the rapidly changing details (fine features) that cause high frequency in the signal while the features that are detected at large scales (stretched wavelet) are the slowly changing details (coarse features) that cause high frequency in the signal.

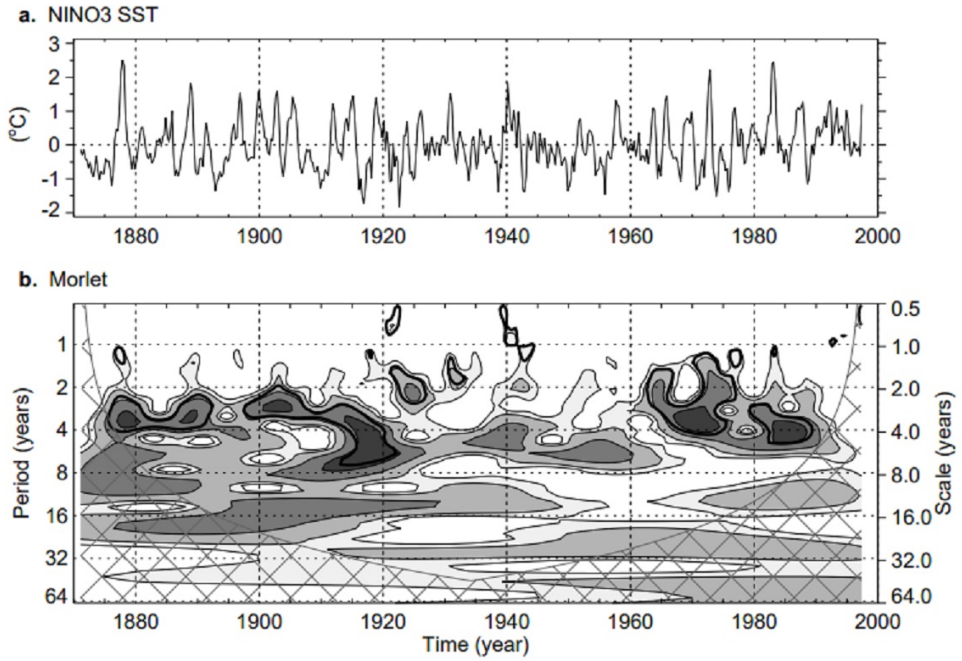


Figure 4. Example for the wavelet transform analysis of the monthly climate temperature (Nino3 SST) time series data: (**a**) The Niño3 SST time series data; and (**b**) the local wavelet power spectrum using the wavelet transform analysis of (**a**) using the Morlet wavelet (Torrence and Compo (1998) [53]).

2.2. CWT Fracture Closure Detection Technique

In this study, a new innovative technique to find a closure pressure using the CWT technique is introduced. The main idea behind estimating the minimum stress using the diagnostic fracture injection test is to create a small fracture at a constant rate and then shut down the pumps and observe the pressure at which the fracture closes. The closure pressure is the minimum average of the minimum stress for the area covered by the fracture created by the DFIT. The pressure during the shut-in and the observation period represents the closure process of the formation. The main goal is to detect and magnify the pressure changes that reflect the fracture's closure event. The pressure signal during the shut-in period after DFIT is analyzed using the CWT technique with a complex Morlet wavelet to obtain the signal energy. The complete workflow for the CWT closure detection technique is shown in Figure 5. The technique starts by getting the coefficient of CWT using the complex Morlet wavelets at multiple scales (from zero up to a scale of 256) and then getting the wavelet transform modulus (WTM) using Equation (3) as a scalogram. The scalogram of signal energy is plotted using a log scale. The scalogram can be averaged to the average of the log signal energy of all scales. Fracture closure as a dominant feature can be identified by the average of all log signal energies at several wavelet scales. The average of the log of signal energy can be plotted with time. The plot can be used to detect the closure event as seen in Figure 5.

Fracture closure can be identified with the two following features: the fracture closure starts with a peak in the average of the log signal energy, which represents the fracture walls coming into contact, then the drop in log signal energy level to a minimum stabilized level, which represents reaching the equilibrium state. The characteristics of fracture closure can be seen in Figure 6. When the real field data are analyzed, high oscillatory signal energy may be observed due to the noise of real field data. That may be due to several reasons, and the fracture faces are not smooth faces and the closure does not happen in subsurface formation instantaneously, or there is noise in the pressure data, or due to that, the equilibrium state is still disturbed with the DFIT.

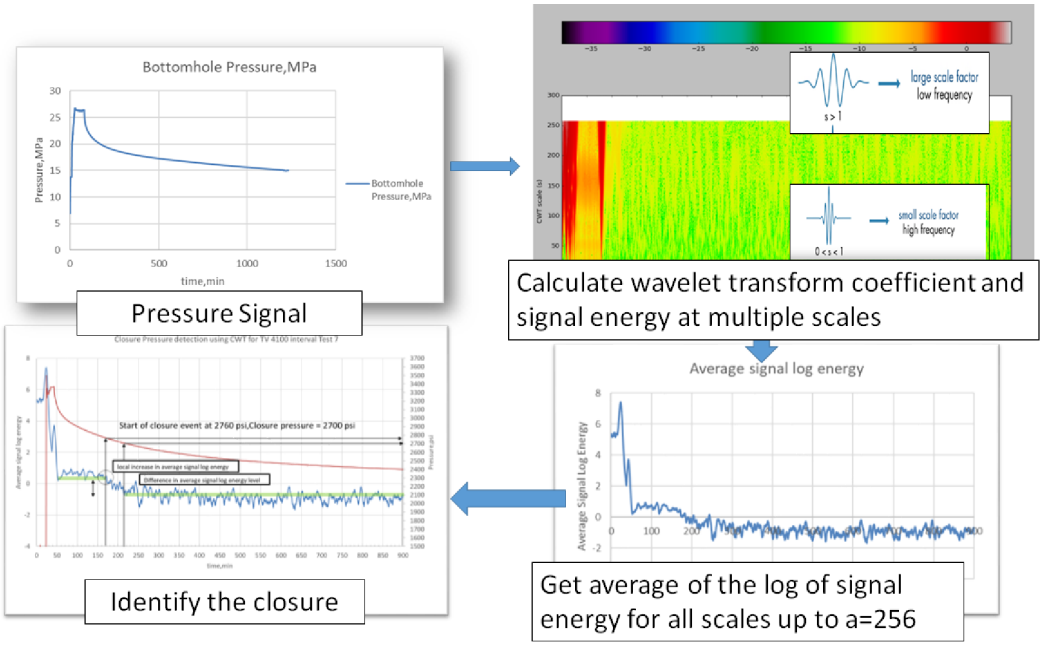


Figure 5. Fracture closure detection workflow using the CWT closure detection technique.

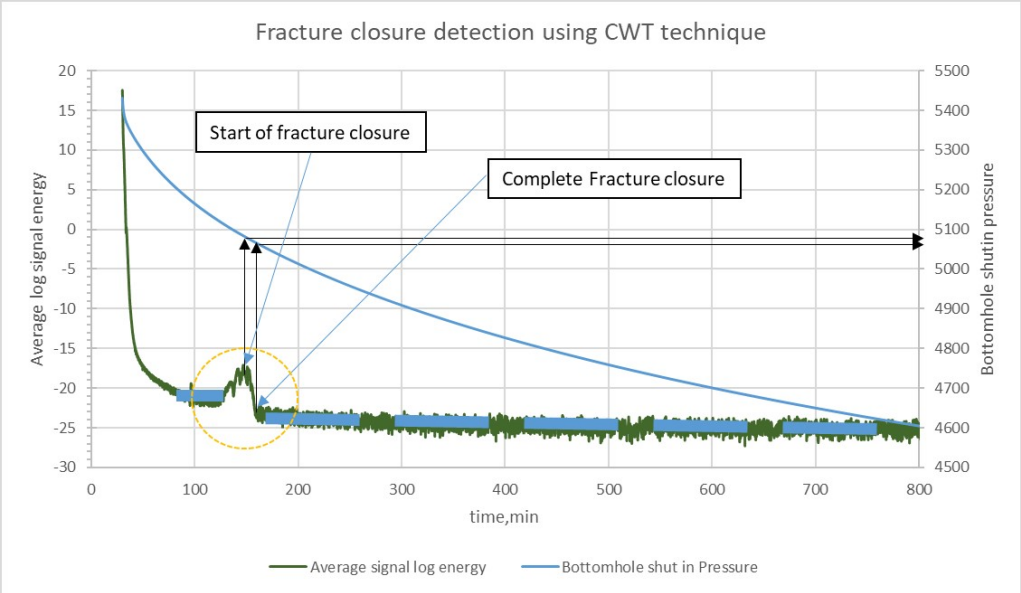


Figure 6. Fracture closure pressure using CWT closure detection technique.

2.3. Summary

The new CWT fracture closure detection technique can be conducted as the following steps: The first step is to apply the CWT using a complex Morlet wavelet for the pressure signal starting from the start of DFIT pumping to obtain the CWT coefficient at different scales up to (a = 256) as per Equation (1) and then obtain the wavelet transform modulus (WTM) as per Equation (4) from the complex continuous wavelet coefficient. This can be followed by the calculation of signal energy using Equation (2). Considering fracture closure is a dominant feature so it can be detected by averaging the log of signal energy values at each time point for different scales (up to scale (a) = 256). From the plotted signal average log energy versus time, the start and the end of the fracture closure event can be identified with the following characteristics. The start of the fracture closure which represents the contact of two fracture faces can be recognized by a peak in average signal log energy at the start of the fracture closure. The fracture closure can be identified by the

drop in signal average log energy level to a minimum stabilized level. The start of the minimum stabilized level characterizes the end of the fracture closure event.

3. Results and Discussion

3.1. Validation Using Fracture Simulation

The numerical simulations in this study were performed using the commercial planar 3D fracture simulator introduced by Barree (1983). The simulator integrates a finite difference formulation for the fluid flow calculation within the fracture with an integral equation for fracture width. Fluid pressure and fracture width solutions are sequentially coupled based on the linear-elastic solution of the deformation for an infinite half-space with a concentrated load. This relies on Poiseuille's equation along with the continuity condition. It uses a pressure-dependent leak-off model for the effect of natural fractures. This simulation is solved using finite differences with a regular grid. The shear-rate and time-dependent laboratory fluid test data are used to model the fluid rheology. Proppant transport is coupled with fluid flow and iteratively solved for proppant distribution in fractures. The simulator is widely used by the oil and gas industry and its fracture geometry is validated by downhole events in a stacked fluvial pay system as per Nur. Azlinda et al. (2010) [12].

To test the new CWT closure detection technique using fracture simulation, grids for the synthetic model are created with ideal properties; the idealized reservoir model has 25 ft. of the sand body between two shale barriers with a sharp stress contrast and constant values for reservoir characteristics and geo-mechanical parameters. High-stress contrast between the pay zone and the surrounding shale zones is assumed. It is assumed that the reservoir is tight (the formation permeability is 5 micro Darcy) and a simulation run was conducted with a fluid volume (10,000 gallons of KCL water) of diagnostic fracture injection test with the typical pumping rate of 8 bbl/min followed by 700 min of leak-off. This is a standard DFIT procedure that is followed by the oil/gas industry. The KCL water is commonly used to prevent clay swelling and it is a non-wall building fluid with viscosity changes with temperatures. The concentration of KCL is dependent on the needed hydrostatic for the DFIT. The pumping rate is selected to be 8 bbl/min as the maximum of the range of the DFIT pumping rate (3–8 bbl/MIN). The geomechanical and reservoir properties are shown in Figure 7. The perforation shot per foot is selected to be six shots per foot. The DFIT pumping schedule is implemented in the fracture simulator as per Figure 8. The simulation model showed fracture propagation followed by complete fracture closure at 153 min when the average width is equal to zero, as shown in Figure 9. The complete closure pressure is 5075 psi as per the fracture simulation.

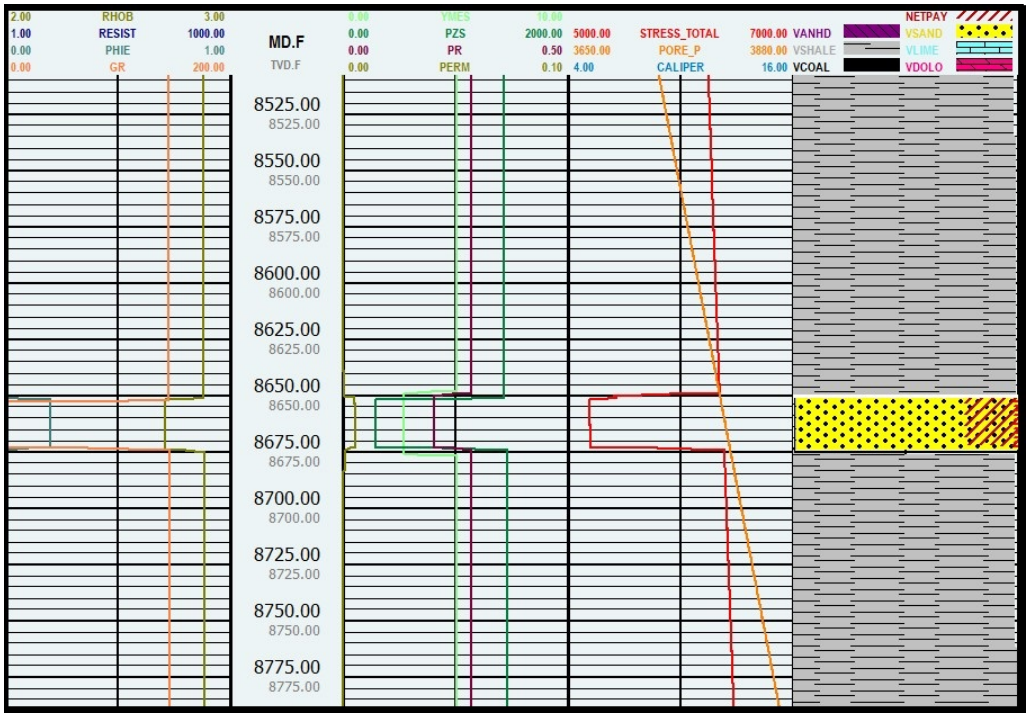


Figure 7. The mechanical Earth model and reservoir properties for the fracture simulation model used to test the CWT closure detection technique.

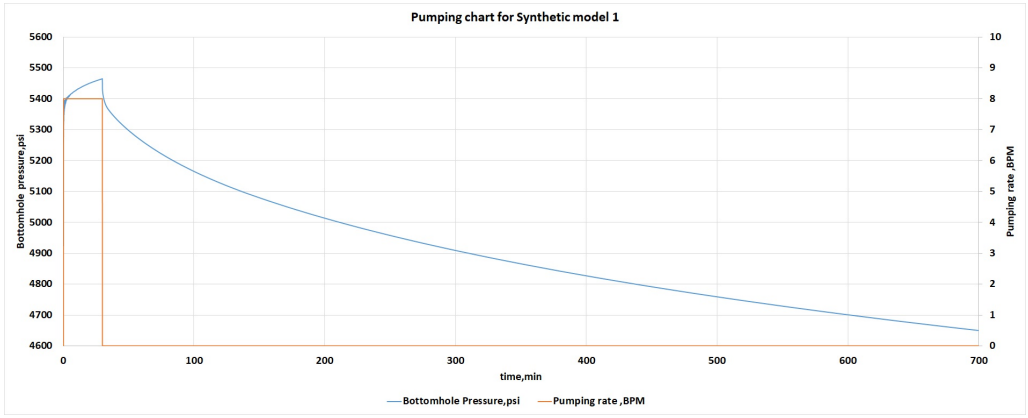


Figure 8. Synthetic model 1 pumping chart.

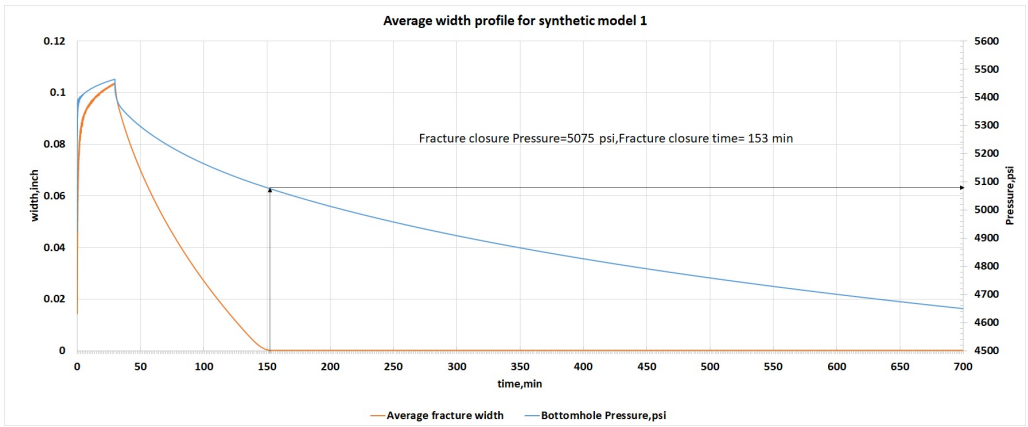


Figure 9. Average width profile for synthetic model 1.

The pressure from the fracture stimulation was analyzed with CWT to obtain the average energy over wavelet scales (up to scale (a) = 256). The average log signal energy was plotted against the time to detect the fracture closure in Figure 10. The energy signal in Figure 10 showed a peak at a time of 149 min which happens at a bottom-hole pressure of 5095 psi. That pressure represents the start of the closure. The complete closure is when the signal average energy drops to a stabilized level. As shown in Figure 10, the CWT technique showed a closure pressure at 5075 psi.

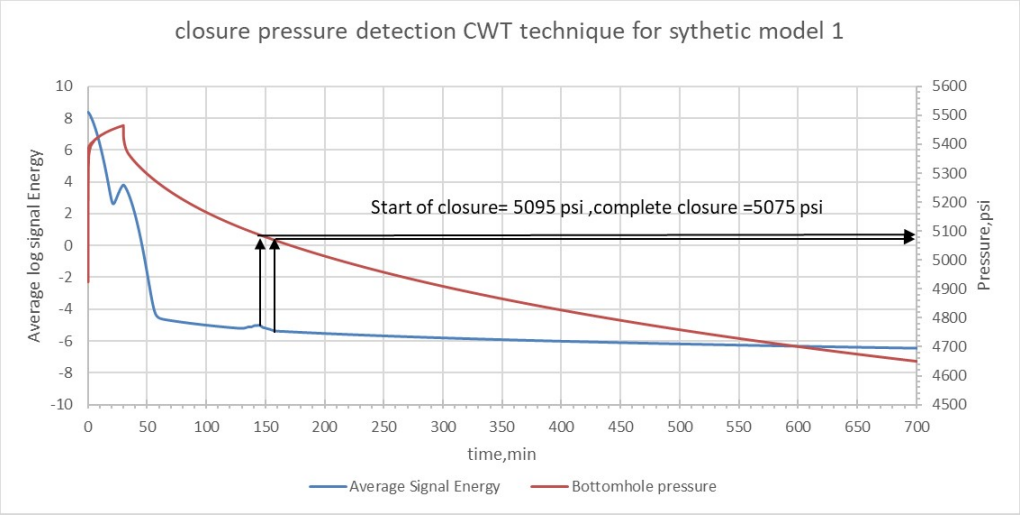


Figure 10. Fracture closure pressure detection using the CWT technique for synthetic model 1.

To understand how the average log signal energy responds to fracture closure, the change in the average width profile created by the fracture simulator is plotted as a semi-log scale against time to magnify the changes in width during the closure. That is to be compared with the average log signal energy to understand how the CWT closure detection technique detected fracture closure. It can be noticed that the difference in the average width profile reached zero at the same time when the average log signal energy reached the stabilized level, as seen in Figure 11.

The limitations of the conventional methods are the assumptions behind each method. For example, the G-function, square root, time, and log–log are based on well-testing concepts, built on a constant pumping rate and shut-in. Therefore, the variable-rate pumping schedule does not ideally fit the basic concepts of these methodologies. However, the introduced CWT closure detection is a technique that does not rely on built-in assumptions. It depends on the wavelet transform acting as a global mathematical microscope to obtain the physical response of the signal. The closure detection technique was tested for a variable pumping rate case. A pumping schedule with a variable pumping rate was simulated using the same ideal homogeneous geomechanical parameters used in Figure 7. The pumping rate started at 4 bbl/min and then increased to 8 bbl/min and finally to 10 bbl/min, as shown in Figure 12. The simulation model showed fracture propagation and then complete fracture closure at 184.5 min, where the average width is equal to zero as shown in Figure 13.

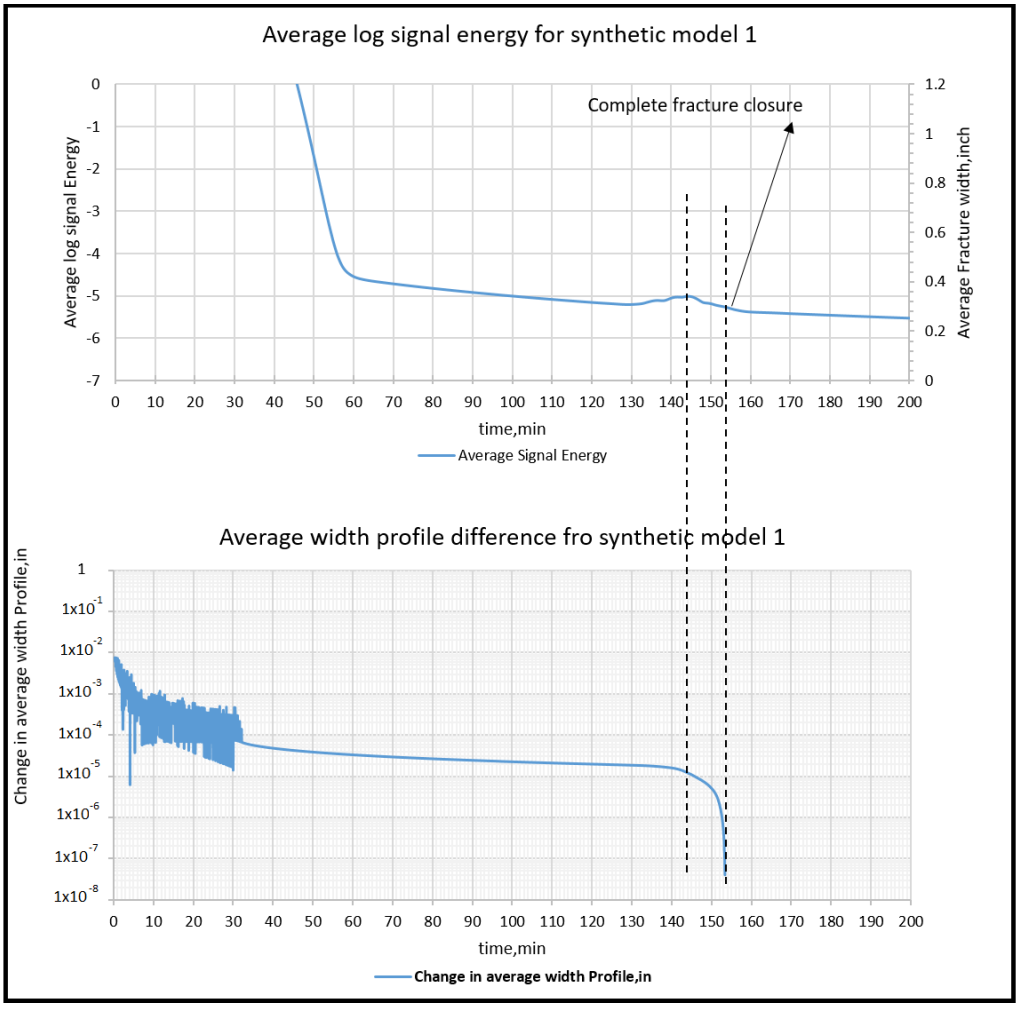


Figure 11. Comparison between the change in average width profile and CWT closure detection technique plot.

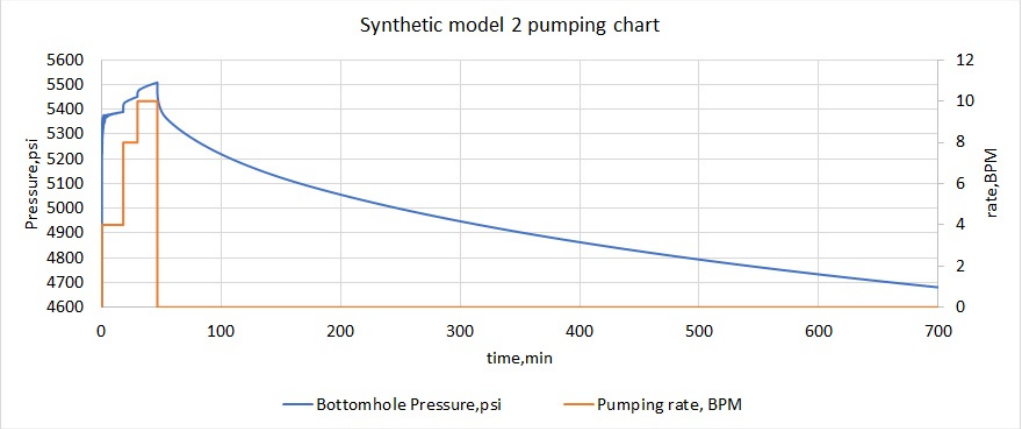


Figure 12. Synthetic model 2 pumping chart.

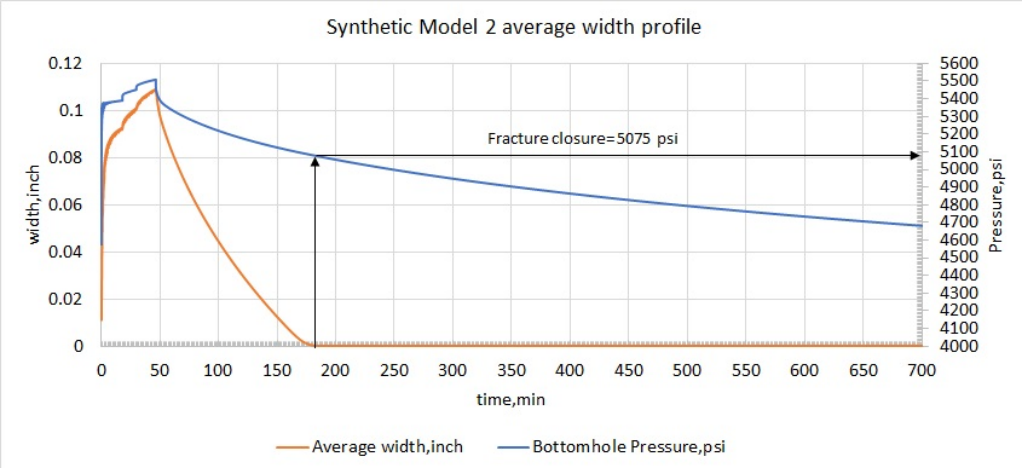


Figure 13. Average width profile for synthetic model 2.

The simulation for synthetic example 2 yielded the same closure pressure of 5075 psi but at a time of 184.5 min. That is what was expected using as the pumping rate changed from the synthetic model 1. The pressure from the fracture stimulation was analyzed with the CWT closure detection technique by plotting the average of the log signal energy against time. From Figure 14, it is clear that the signal energy showed a peak at 169 min, representing the bottom hole pressure of 5095 psi, which represents the start of the closure process. The complete closure pressure is at the moment when the signal average energy drops to a stabilized level at a time of 184.5 min (closure pressure = 5075 psi). As shown in Figure 14, the CWT analysis yielded a closure pressure at 5075, the fracture closure is the same as in the first synthetic model since the geomechanical parameters are the same. However, the closure time changed due to a change in the pumping rate and fluid volume.

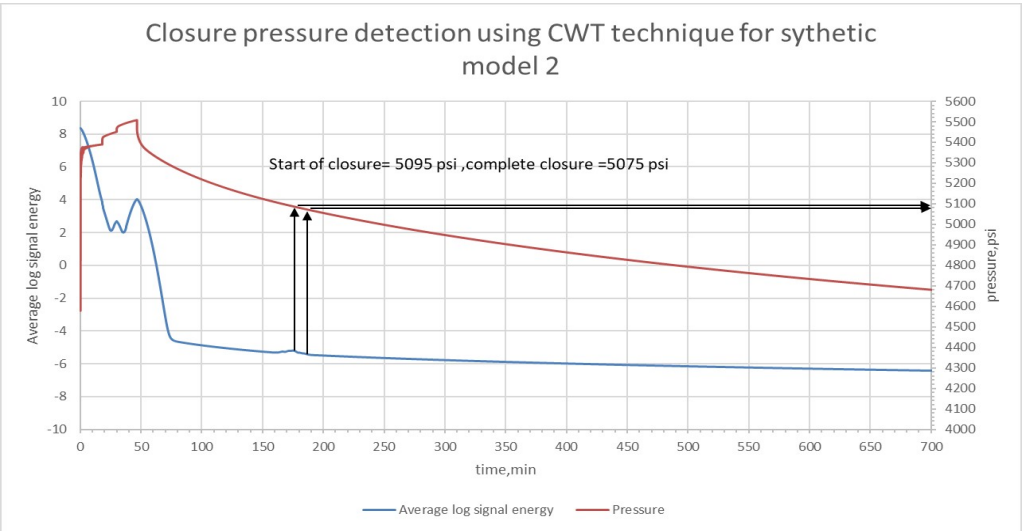


Figure 14. Signal average log energy using CWT for synthetic model 2.

3.2. Validation Using Flow Regime Modeling

To further test the new technique with the complicated nature of the fracture closure, a new approach was developed. This approach may be used to validate the CWT technique using flow regime modeling with a synthetic pressure decay signal that has no noise and represents the characteristic flow regimes that happen before and after fracture closure. The flow regime is identified by the rate of change in pressure with time. A set of flow regimes were assumed to obtain a synthetic pressure leak-off signal that has a rate of change in pressure representing those flow regimes, then the wavelet transform technique was tested

to know how the CWT closure detection technique detects the closure. Various pre-closure and post-closure flow regimes can be identified on the log–log Δt dΔp /dΔt versus Δt plot. Table 1 shows the flow regimes that happen pre-closure and post-closure and their corresponding slopes on the log–log ΔtdΔp /dΔt versus Δt. The basic concept can be visualized as given in Figure 15. Table 1 the flow regimes that happen pre-closure and post-closure and their corresponding slopes on the log–log Δt dΔp /dΔt versus Δt.

Table 1. The flow regimes that happen pre-closure and post-closure and their corresponding slopes on the log–log Δt dΔp /dΔt versus Δt.

The Slope of the log–log Δt dΔp/dΔt vs. Δt	Flow Regime
Half slope (1/2)	Pre-closure Linear flow regime
Quarter slope (1/4)	Pre-closure bilinear flow regime
Negative half-slope (−1/2)	Post-closure linear flow regime
Negative three-fourth slope (−3/4)	Post-closure bilinear flow regime
Negative unit slope (−1)	Post-closure pseudo radial flow regime

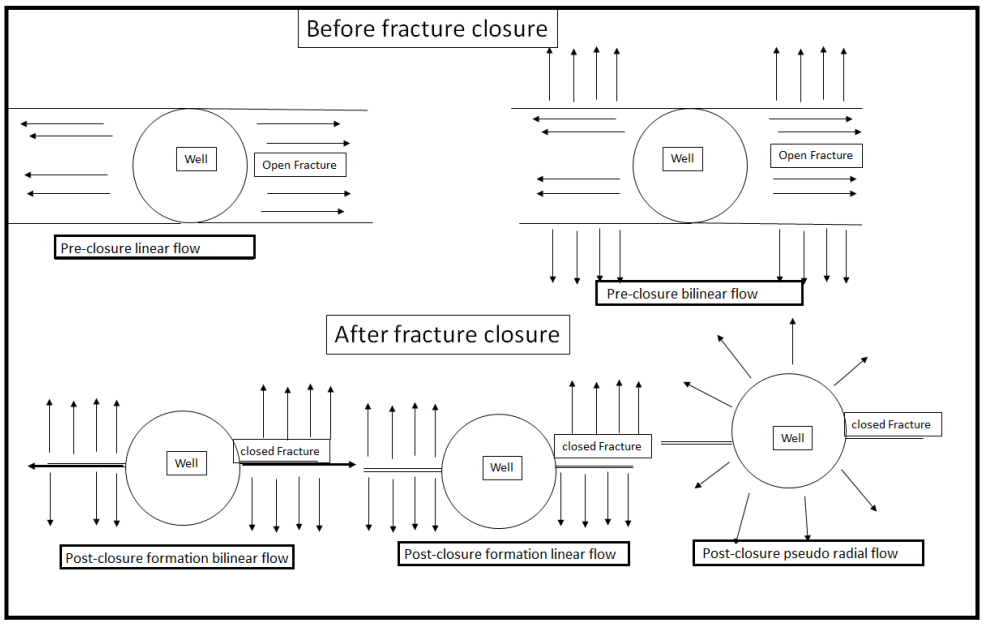


Figure 15. Transient flow regimes before and after fracture closure.

Pre-closure and post-closure flow regimes can be identified using the semi-log pressure derivative on the log–log plot of Δp vs. Δt during the shut-in period following the fracture injection test. A pseudo linear flow period is identified by parallel (1/2) slope lines on the log–log Δp Δt and Δt dΔp/dΔt Δt plot up until fracture closure as seen in Figure 16a,b. Bilinear flow can be identified by parallel (1/4) slope lines on log–log Δpwf versus Δt and Δt d Δp/d Δt versus Δt prior to fracture closure as seen in Figure 16c.

After closure, the pseudo linear formation flow period is identified by a (−1/2) slope of the semi-log derivative of the pressure difference on the same plot, and pseudo radial flow is identified by a (−1) slope of the semi-log derivative on the log–log plot, as seen in Figure 16a,b. It is difficult to obtain all the flow regimes in one real field case. Thus, the perfect fracture closure log–log plot can be synthetically created assuming flow regime slopes and then calculating the pressure decay signal as seen in Figure 17. The slopes that were assumed are the slopes of the log–log plot of Δt dΔp/dΔt vs. Δt for each period of pressure decay signal are shown in Table 2.

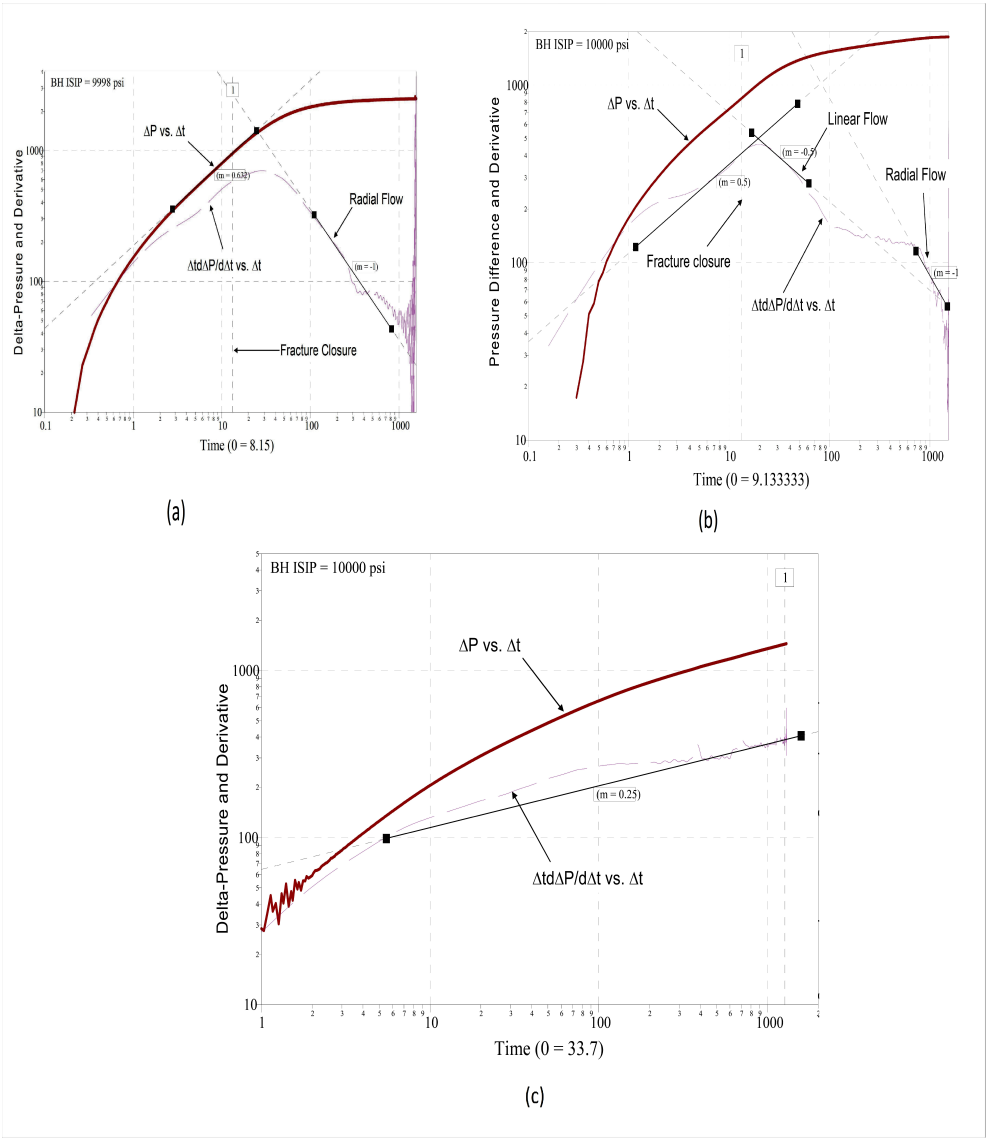


Figure 16. (**a**) Normal leak off log–log plot; (**b**) pressure-dependent leak off log–log plot; and (**c**) tip extension log–log plot (Barree et al. (2009) [26]).

Table 2. The slopes of the log–log plot of Δt dΔP/dΔt vs. Δt for the reverse-calculated pressure decay signal.

Start, min.	End, min.	The Slopes of the log–log Plot of Δt dΔP/dΔt vs. Δt	Pressure at Start, psi.	Pressure at End, psi.
0	5	Pumping period	Pumping period	Pumping period
5	15	0.3	12,000	11,692
15	40	0.5	11,692	11,499
40	50	0.25	11,499	11,445
50	200	−0.5	11,445	11,216
200	360	−1	11,216	11,168

The pressure decay signal and its corresponding flow regimes are shown in Figure 17. The synthetic pressure decay signal can be used to illustrate that the wavelet transform detects the features within the signal itself and not only the noise associated with it. It can also be used to investigate the response of each closure detection technique. The synthetic pressure decay signal was analyzed using each technique as if it was real field data.

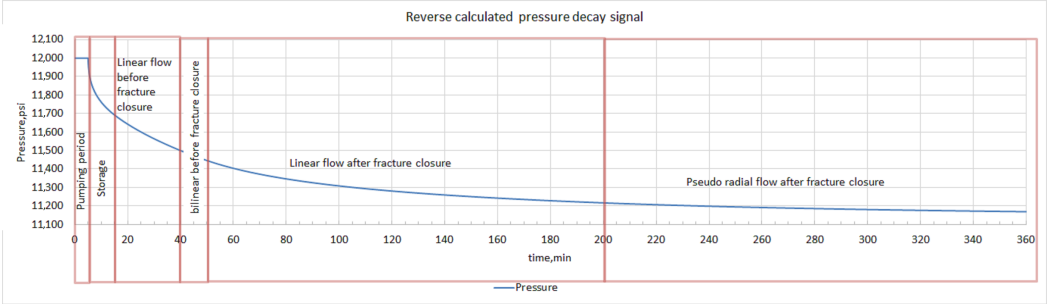


Figure 17. Synthetic reverse-calculated pressure decay signal.

The application of the conventional technique, the tangent method (Barree et al. (2009) [26]), showed that dP/dG monotonically decreases so it can be either rapid closure or it is not valid to be analyzed using the compliance method (Mcclure et al. (2022) [48]). However, the effective shut-in pressure is 11,850 psi which is delayed from the pump shut-down time by a minute and a half. There is no rise in dP/dG. The tangent method using GdP/dG detected the closure pressure at 11,445 psi which represents the end of the linear pre-closure flow regime. The dP/dG and GdP/dG are shown in Figure 18. The pre-closure bilinear flow regime is ignored by the tangent method. The application of the CWT closure detection technique detected the closure at the same point of the change from the bilinear flow regime to the after-fracture-closure linear flow regime. It accurately detected the transition period between pre-closure and post-closure, as can be seen in Figure 19. The fracture closure is usually identified at the end of the pre-closure linear flow, but this is not accurate as the pre-closure bilinear flow can be detected in several real field cases. However, that bilinear flow period is very short and cannot be observed in many real field cases. CWT closure detection technique detected the transition between pre-closure and post-closure with a clear peak. The change in flow regime between the pre-closure and post-closure periods can also be identified with smaller and smoother peaks. The closure pressure detected using the CWT technique matches the most accurate definition of complete fracture closure.

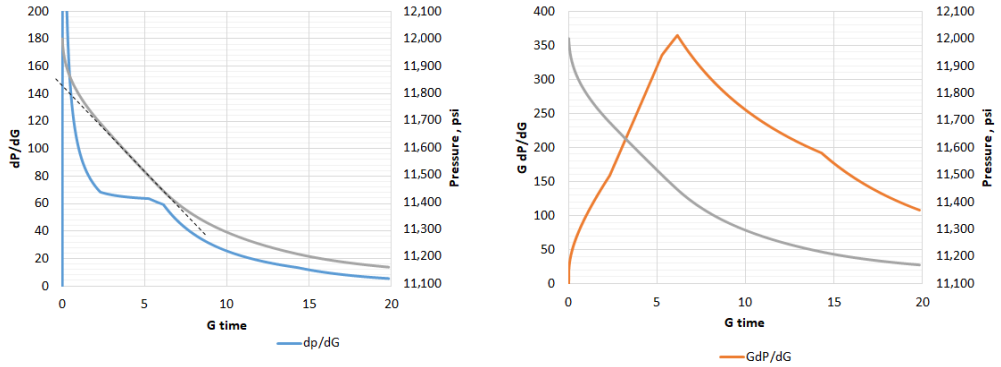


Figure 18. Tangent method (dP/dG and GdP/dG) for the synthetic reverse-calculated pressure decay signal.

The large peak matches the closure process as seen in Figure 19. This is when the fracture closes and the flow starts to follow a formation linear flow regime. This includes the period of bilinear flow where the formation and fracture flow together and each of them

shows a linear flow regime. The multiple peaks that are shown in the reverse-calculated pressure decay signal are not shown in fracture simulation synthetic data as the fracture simulation did not include the post-closure reservoir flow regimes. It only simulates hydraulic fracture propagation and closure.

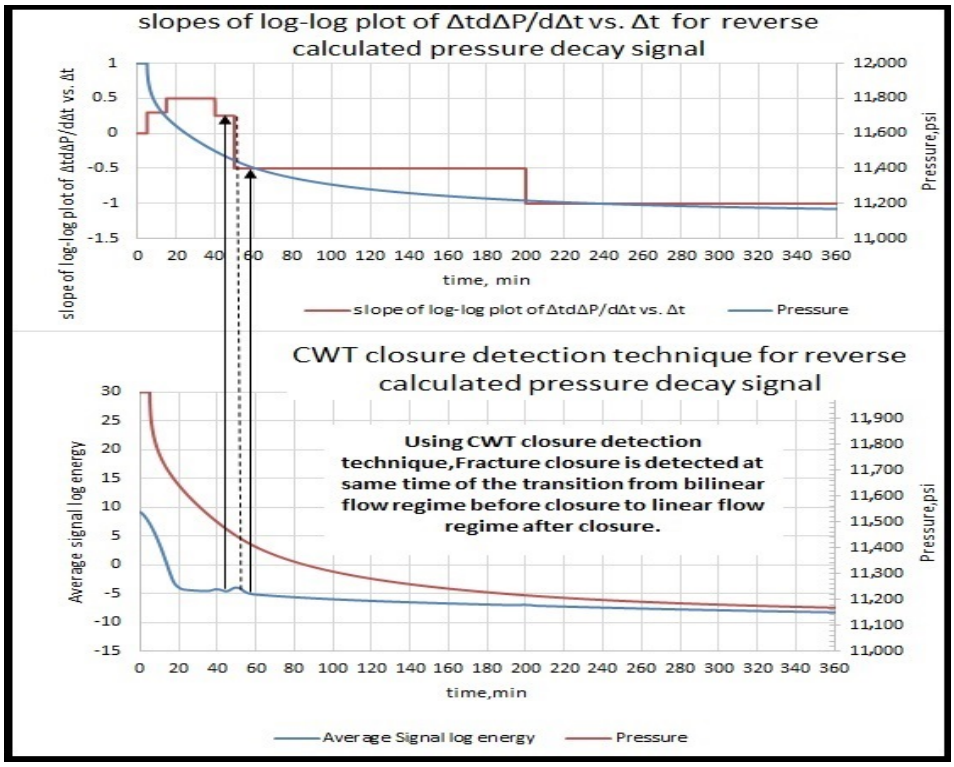


Figure 19. Closure pressure detection using the CWT technique for the synthetic reverse-calculated pressure decay signal.

3.3. Application of CWT on Real Field Data

The main challenge for any technique is to be applied to real field data. We compared the closure pressure of a real field DFIT case estimated using the CWT technique to the conventional methods such as the tangent method, log–log, and square root of the time and compliance methods. This was performed to determine how the CWT closure detection technique stands up against other techniques used in the industry. Thus, two real field cases, wells X-01 and X-02 were selected for the analysis of the new CWT technique. The well X-01 was perforated against a conventional oil sandstone reservoir. The well X-02 was perforated against a deep high temperature (400 degrees Fahrenheit) granite reservoir as a conventional example for geothermal energy reservoirs. The well X-01 was perforated through a sandstone formation. One thousand gallons of water were pumped at a rate of 8 bbl/min through a 10 ft perforated interval as a typical DFIT pumping schedule. This was selected as the well site by the operating company. The pressure fall-off was observed for 110 min, as shown in Figure 20. The CWT closure detection technique showed that the closure started at a pressure of 7400 psi (start of closure) and ended at 6600 psi (complete closure). As shown in Figure 21, the start of closure can be distinguished by increased energy levels followed by a drop in the average of signal log energy. The complete closure pressure is when the level of energy drops to a lower level. The oscillatory signal energy with real field data may be due to the complexity of fracture closure in addition to the presence of noise in the pressure signal observed in real field data.

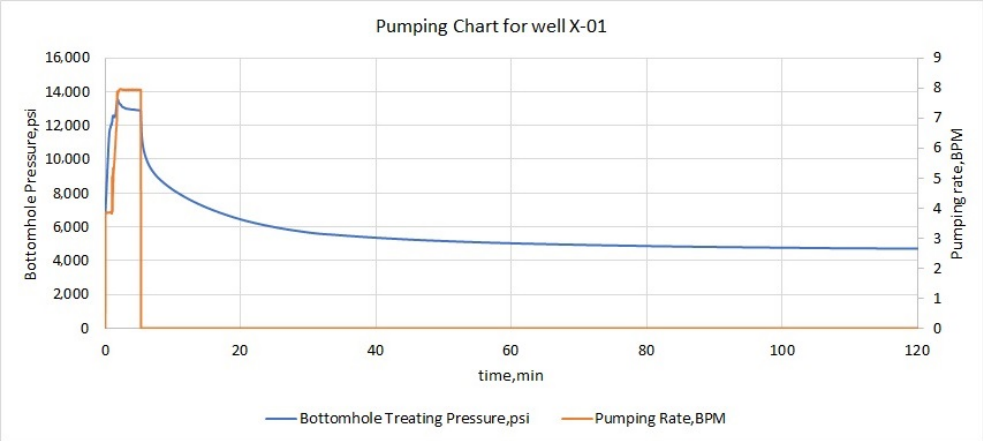


Figure 20. Pumping chart for well X-01.

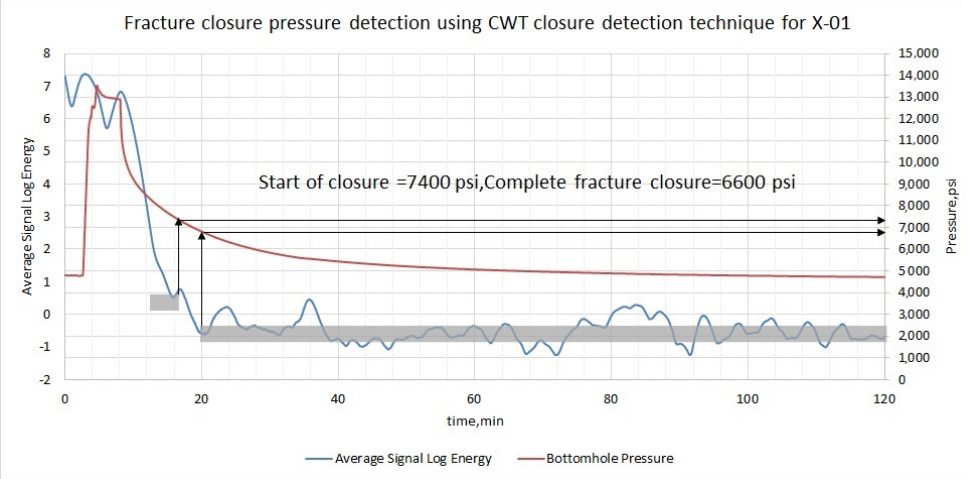


Figure 21. Closure pressure detection using CWT closure detection technique for well X-01.

Application of classical conventional methods, tangent method (Barree et al. (2009) [26]), showed that closure pressure is the same as what the CWT closure detection technique detected. The closure pressure is 6600 psi as per the tangent method shown in Figure 22. The log–log technique detected the closure at the same pressure (6600 psi). The closure pressure is the point at which the fracture linear flow ended (slope of 0.5 at $\Delta t d\Delta p/d\Delta t$ vs. Δt log–log plot) and the formation linear flow started (slope of -0.5 at $\Delta t\, d\Delta p/d\Delta t$ vs. Δt log–log plot) as shown in Figure 23. The square root of the time method detected the closure at the same point of 6600 psi, as seen in Figure 24. The compliance method (Mcclure et al. (2022) [48]) using dP/dG vs. G-time plot did not show a clear signature for the closure. There is no rise-up in dP/dG, as shown in Figure 22. However, there is a zero slope period at a pressure of approximately 7700 psi which can be defined as a closure. According to McClure et al. (2019) [46], the DFIT is invalid due to the high near-wellbore tortuosity or the fracture may appear to be closed earlier than it should. The closure pressure value picked by the CWT technique matched the classical closure detection techniques. In addition to that, CWT showed both the start and end of the fracture closure period. Table 3 lists the closure pressure detected using each methodology for well X-01. The closure detected using the CWT technique only used the pressure decline data without any information about the pumping period or formation properties. In the well X-01 case, the CWT technique was applied to analyze the classic DFIT in a conventional sandstone formation. However, it was also tested on a very tight reservoir. The well X-02 was perforated through granite formation, which is the typical geothermal formation type, and then pumped the DFIT as per the pumping schedule shown in Figure 25.

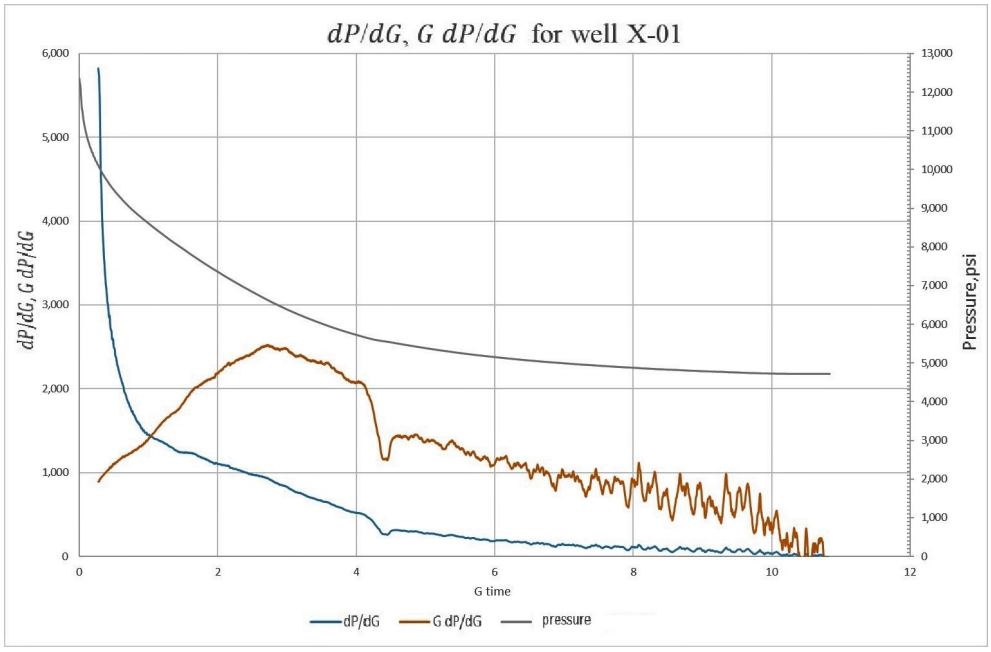


Figure 22. Tangentmethod (dP/dG and GdP/dG) for well X-01.

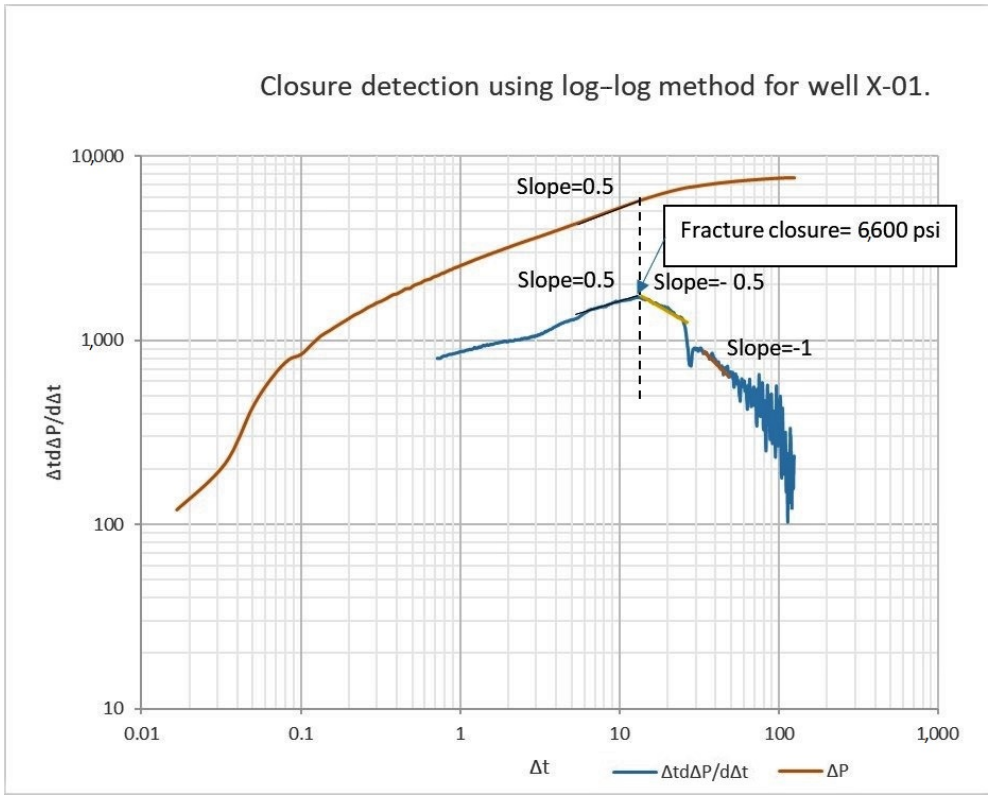


Figure 23. Closure detection using the log–log method for well X-01.

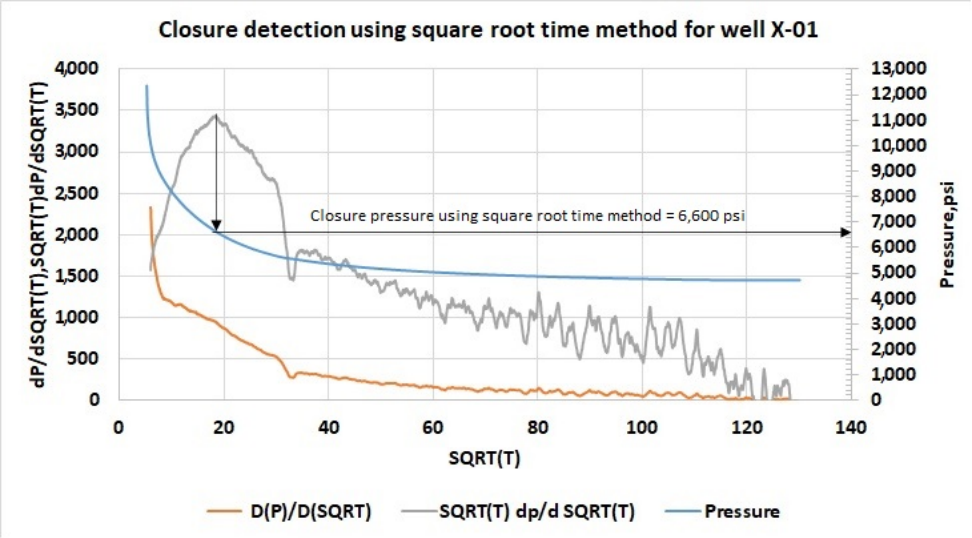


Figure 24. Closure detection using the square root time method for well X-01.

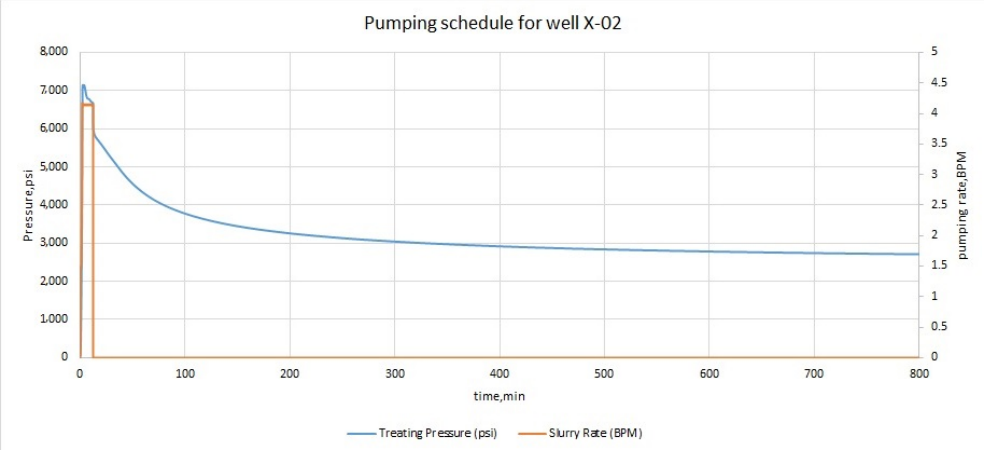


Figure 25. Pumping schedule for well X02.

Table 3. Fracture closure pressure for well X-01.

Method	Closure Pressure,psi
Tangent method (G-function) technique	6600 psi
Log–log technique	6600 psi
Square-root time technique	6600 psi
Compliance method	Invalid DFIT
CWT fracture closure detection technique	Start of fracture closure = 7400 psi, complete fracture closure = 6600 psi

The application of the CWT closure detection technique showed oscillatory signal energy. That may be due to a noise in the pressure signal recorded during the shut-in period or the presence of natural fractures in granite formations. The presence of natural fractures is confirmed with the image log of the well as shown in Figure 26. Natural fractures may cause noise and aggressive fluctuations in the pressure decay signal. The CWT technique detected the start of fracture closure at the pressure of 5300 psi and complete fracture closure to be 4700 psi, as shown in Figure 27. The application of the tangent method (Barree et al. (2009) [26]) using GdP/dG showed fracture closure at the same complete fracture closure that the CWT technique detected (4700 psi), as shown in Figure 28. This was confirmed

by the square root of time, as seen in Figure 29. However, the log–log plot showed the fracture closure at 4523 psi, as seen in Figure 30. The closure pressure is detected at the end of before the closure bilinear flow regime. The application of the compliance method (Mcclure et al. (2022) [48]) showed the contact pressure to be 5625 psi as the dP/dG starts to rise up from the minimum at 5700 psi so the contact pressure is at 75 psi of that pressure, as seen in Figure 28. The main advantage of the CWT technique is that it illustrates the conflict between the tangent methods and the holistic fracture diagnostic technique and captured the full image of the fracture closure process. Table 4 showed the comparison between various techniques for well X-02.

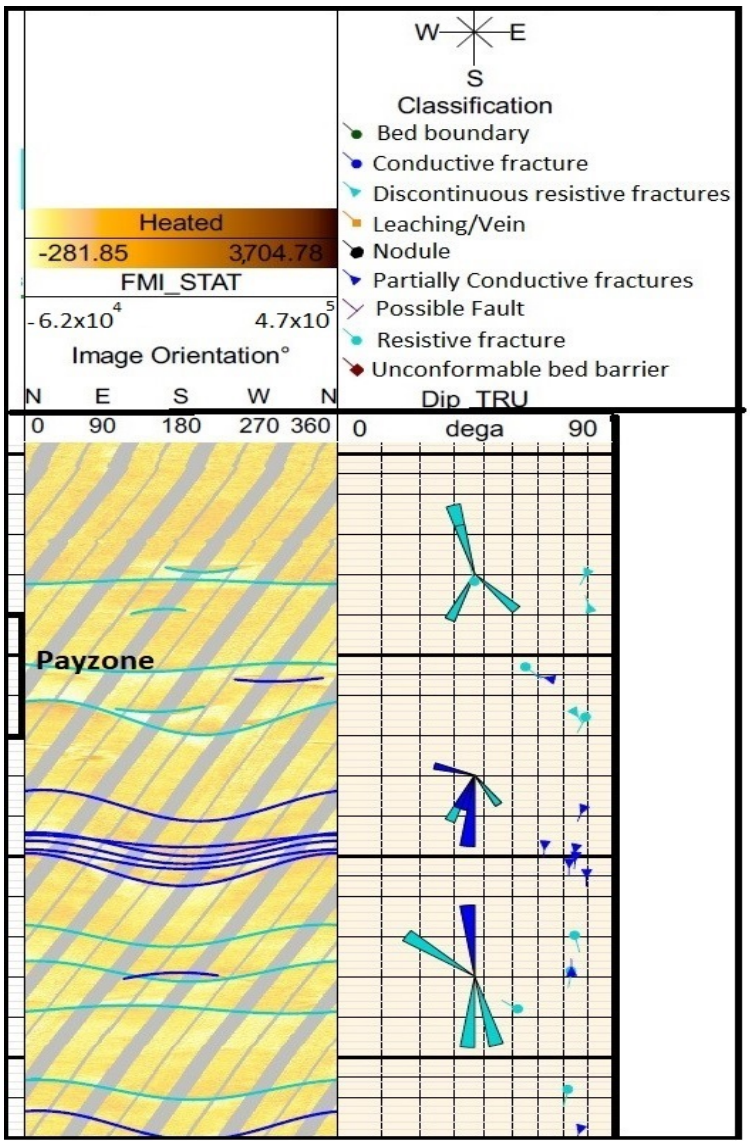


Figure 26. Formation image log for well X-02 indicating the presence of natural fractures in the granite reservoir.

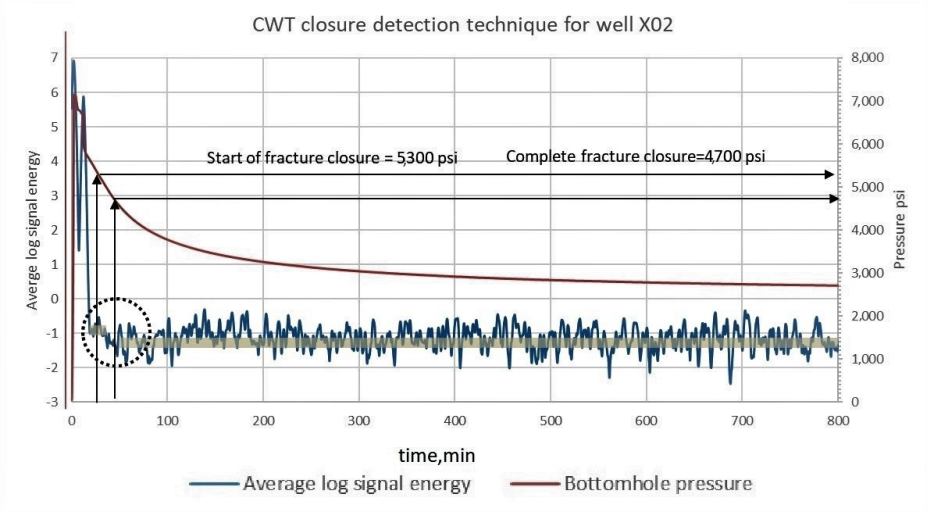


Figure 27. Closure identification using a CWT closure detection technique for well X02.

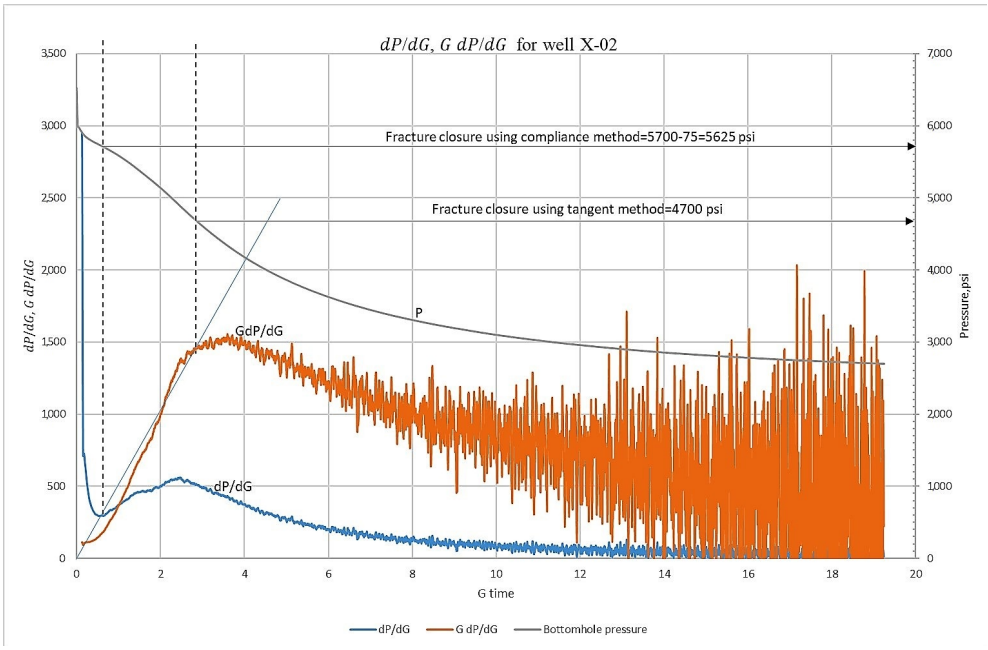


Figure 28. Tangent method (dP/dG and GdP/dG) for well X-02.

With the application of the CWT closure detection technique on real data cases, fracture closure can be detected at a lower maximum scale or higher maximum scale than that used in the study (a = 256) based on the noise of the data and the time of the signal. The selected maximum scale is iterative until fracture closure is identified. The signal energy scalogram can be used as a guide for the maximum value for the maximum scale used. That is because when the scale (wavelet scale (a)) increases more than required, it can miss the fracture closure event. The value for the maximum scale (wavelet scale (a)) may depend on several factors such as the length of the pressure decay signal, the complexity and the duration of fracture closure, and the level of noise that is in the pressure decay signal.

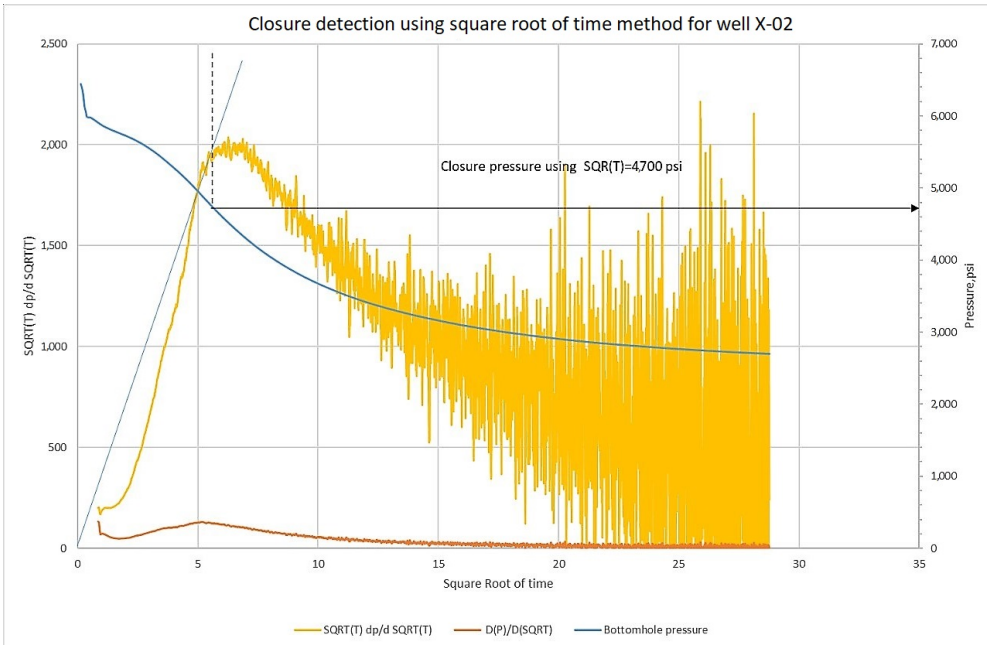


Figure 29. Closure identification using the square root of time technique for well X-02.

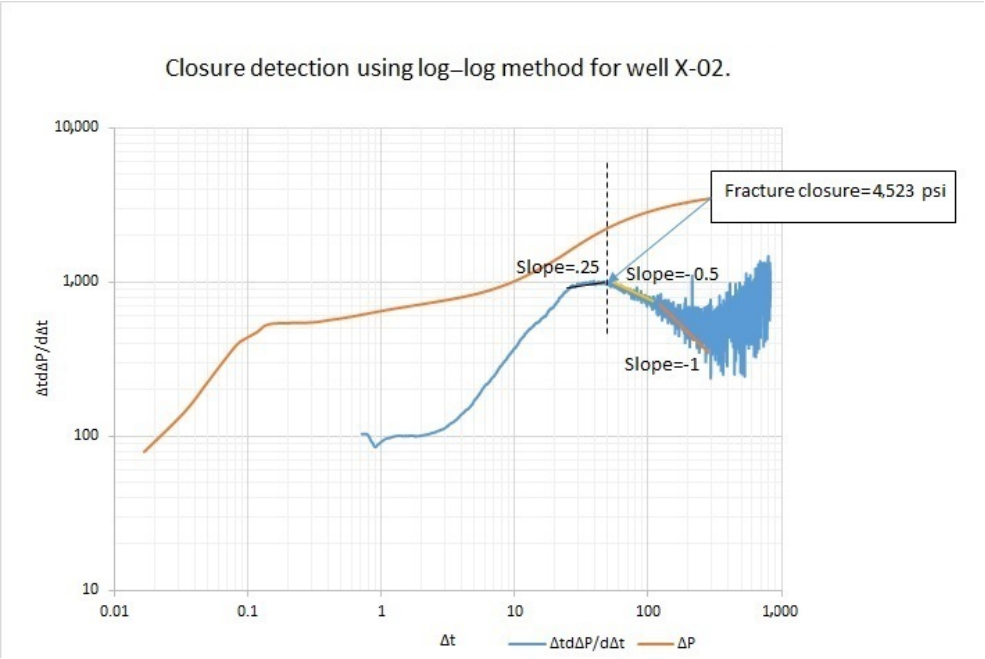


Figure 30. Closure detection using the log–log analysis technique for well X-02 (closure identified when the slope of changes from 1/4 (pre-closure bilinear flow) to −1/2 (post-closure formation linear)).

Table 4. Fracture closure pressure for well X-02.

Method	Closure Pressure, psi
Tangent method (G-function) technique	4700 psi
Log–log technique	4523 psi
Square-root of time technique	4700 psi
Compliance method	5625 psi
CWT fracture closure detection technique	Start of fracture closure = 5300 psi, complete fracture closure = 4700 psi

4. Conclusions

CWT can be used as a general mathematical microscope to analyze the output of the physical systems (i.e., the diagnostic fracture injection test) to understand the process of fracture closure. That can be used for multiple purposes in oilfield operations and geothermal reservoir operations. Time–frequency analysis for a pressure decay signal using CWT reliably detects the closure pressure. The following conclusions can be concluded from previous discussions:

1. The average of the log signal energy versus time calculated using CWT characterizes the closure event as a local increase in the signal log energy followed by a drop in the signal log energy to a minimum stabilized level.
2. The proposed technique has shown good agreement with synthetic fracture simulator data.
3. The application of the CWT technique matched the classical closure detection techniques in real field cases with no pre-assumptions and less available data.
4. The pressure decay signal reflects the physical process of fracture closure and the average signal energy using CWT is just a mathematical independent magnification for the pressure decay.
5. The start of the fracture closure can be identified with the CWT closure detection technique at the local peak of average signal energy. Fracture closure ends when the average signal energy reaches the minimum stabilized level. Those characteristics matched numerical simulation, flow regime modeling, and real field cases. The technique is consistent, reliable, and can efficiently detect fracture closure.
6. The CWT closure detection technique can be used to analyze the real field data and can detect a reliable closure pressure compared to current methods.
7. The CWT closure detection technique can detect fracture closure regardless of the noise that may accompany the real field pressure signal, it showed accurate fracture closure in synthetic data when there was no noise included in the pressure decay signal.
8. The new technique has no built-in assumptions and works on the pressure decay signal during the shut-in period.
9. Using CWT to detect the closure can be generalized to detect the features from oilfield signals such as rate, torque, and drilling vibrations. Another perspective of the CWT closure detection technique is using the CWT wavelet transform to investigate the natural fracture in the subsurface formations.

5. Patents

This study was filed under U.S. Patent Application No. 63/412,269 on 30 September 2022, and entitled "SYSTEMS AND METHODS FOR MONITORING SUBSURFACE EVENTS USING CONTINUOUS WAVELET TRANSFORMS."

Author Contributions: Conceptualization, M.A.G. and I.E.; methodology, M.A.G.; software, I.E.; validation, I.E.; supervision, M.Y.S. and S.M.F.-A.; writing—original draft, M.A.G. and I.E.; writing—review and editing, M.Y.S. and S.M.F.-A. All authors have read and agreed to the published version of the manuscript.

Funding: This research received funding from HESS Corporation, Shell PLC, and Halliburton Energy Service, members of the hydraulic fracturing consortium at the University of Houston.

Institutional Review Board Statement: Not applicable.

Informed Consent Statement: Not applicable.

Data Availability Statement: The data presented in this study are available on request from the corresponding author.

Acknowledgments: We thank HESS Corporation, Shell PLC, and Halliburton Energy Service, members of the hydraulic fracturing consortium at the University of Houston, for sponsoring this work.

Conflicts of Interest: The authors declare no conflict of interest.

Abbreviations

The following abbreviations are used in this manuscript:

Δt	Shut in time
a	Dilation parameter or scale
b	Transportation parameter
CWT	Continuous wavelet transform
DFIT	Diagnostic fracture injection test
DWT	Discrete wavelet transform
FT	Fourier transform
G	G-time function
P	Pressure
t	Time
T	Wavelet transform modulus
WFT	Windowed Fourier transform
WT	Wavelet transform

References

1. Eaton, B.A. Fracture gradient prediction and its application in oilfield operations. *J. Pet. Technol.* **1969**, *21*, 1353–1360. [CrossRef]
2. Blanton, T.; Olson, J.E. Stress magnitudes from logs: Effects of tectonic strains and temperature. *SPE Reserv. Eval. Eng.* **1999**, *2*, 62–68. [CrossRef]
3. Zain-Ul-Abedin, M.; Henk, A. Building 1D and 3D Mechanical Earth Models for Underground Gas Storage—A Case Study from the Molasse Basin, Southern Germany. *Energies* **2020**, *13*, 5722. [CrossRef]
4. Xing, P.; McLennan, J.; Moore, J. In-Situ Stress Measurements at the Utah Frontier Observatory for Research in Geothermal Energy (FORGE) Site. *Energies* **2020**, *13*, 5842. [CrossRef]
5. Germán-Salló, Z.; Strnad, G. Signal processing methods in fault detection in manufacturing systems. *Procedia Manuf.* **2018**, *22*, 613–620. [CrossRef]
6. Soliman, M.; Ansah, J.; Stephenson, S.; Mandal, B. Application of wavelet transform to the analysis of pressure-transient data. *SPE Reserv. Eval. Eng.* **2003**, *6*, 89–99. [CrossRef]
7. Unal, E.; Siddiqui, F.; Soliman, M.; Dindoruk, B. Wavelet analysis of DFIT data to identify fracture closure parameters. In Proceedings of the SPE Hydraulic Fracturing Technology Conference and Exhibition, The Woodlands, TX, USA, 5–7 February 2019.
8. Awad, M.M.; Eltaleb, I.; Mansi, M.; Rezaei, A.; Soliman, M.; Farouq-Ali, S.; Dindoruk, B. Interpretation of Hydraulic Fracturing Events by Analyzing the Energy of Rate and Pressure Signals. In Proceedings of the SPE Annual Technical Conference and Exhibition, Virtual, 27–29 October 2020.
9. Eltaleb, I.; Rezaei, A.; Siddiqui, F.; Awad, M.; Mansi, M.; Dindoruk, B.; Soliman, M. Analysis of fracture injection tests using signal processing approach. In Proceedings of the SPE/AAPG/SEG Unconventional Resources Technology Conference, Virtual, 20–22 July 2020.
10. Eltaleb, I.; Rezaei, A.; Soliman, M.; Dindoruk, B. A signal processing approach for analysis of fracture injection test in geothermal reservoirs: A case study on the utah FORGE formation. In Proceedings of the SPE Hydraulic Fracturing Technology Conference and Exhibition, Virtual, 4–6 May 2021.
11. Barree, R. A practical numerical simulator for three-dimensional fracture propagation in heterogeneous media. In Proceedings of the SPE Reservoir Simulation Symposium, San Francisco, CA, USA, 15–18 November 1983.
12. Mohammad, N.A.; Miskimins, J.L. A Comparison of Hydraulic-Fracture Modeling With Downhole and Surface Microseismic Data in a Stacked Fluvial Pay System. *SPE Prod. Oper.* **2012**, *27*, 253–264. [CrossRef]
13. Clark, J. A hydraulic process for increasing the productivity of wells. *J. Pet. Technol.* **1949**, *1*, 1–8. [CrossRef]
14. Hubbert, M.K.; Willis, D.G. Mechanics of hydraulic fracturing. *Trans. AIME* **1957**, *210*, 153–168. [CrossRef]
15. Godbey, J.; Hodges, H. Pressure measurements during formation fracturing operations. *Trans. AIME* **1958**, *213*, 65–69. [CrossRef]
16. Kehle, R.O. The determination of tectonic stresses through analysis of hydraulic well fracturing. *J. Geophys. Res.* **1964**, *69*, 259–273. [CrossRef]
17. Haimson, B.; Fairhurst, C. Initiation and extension of hydraulic fractures in rocks. *Soc. Pet. Eng. J.* **1967**, *7*, 310–318. [CrossRef]
18. Hickman, S.H.; Zoback, M.D. The interpretation of hydraulic fracturing pressure-time data for in situ stress determinations. In*Workshop on Hydraulic Fracturing Rock Stress Measurements*; National Academy Press: Washington, DC, USA; 1981; pp. 103–127.
19. Nolte, K.G. Determination of fracture parameters from fracturing pressure decline. In Proceedings of the SPE Annual Technical Conference and Exhibition, Las Vegas, NV, USA, 23–26 September 1979.
20. Roegiers, J.-C.; McLennan, J.D.; Schultz, L.D. In-Situ Stress Determinations In Northeastern Ohio. In Proceedings of the 23rd U.S. Symposium on Rock Mechanics (USRMS), Berkeley, CA, USA, 25–27 August 1982.
21. Mayerhofer, M.; Economides, M. Permeability estimation from fracture calibration treatments. In Proceedings of the SPE Western Regional Meeting, Anchorage, Alaska, 26–28 May 1993.

22. Castillo, J. Modified fracture pressure decline analysis including pressure-dependent leakoff. In Proceedings of the SPE/DOE Joint Symposium on Low Permeability Reservoirs, Denver, CO, USA, 18–19 May 1987.
23. Barree, R.; Mukherjee, H. Determination of pressure dependent leakoff and its effect on fracture geometry. In Proceedings of the SPE Annual Technical Conference and Exhibition, Denver, CO, USA, 6–9 October 1996.
24. Mayerhofer, M.; Ehlig-Economides, C.; Economides, M. Pressure transient analysis of fracture calibration tests. *J. Pet. Technol.* **1995**, *47*, 229–234. [CrossRef]
25. Craig, D.P.; Brown, T.D. Estimating pore pressure and permeability in massively stacked lenticular reservoirs using diagnostic fracture-injection tests. In Proceedings of the SPE Annual Technical Conference and Exhibition, Houston, TX, USA, 3–6 October 1999.
26. Barree, R.D.; Barree, V.L.; Craig, D. Holistic fracture diagnostics: Consistent interpretation of prefrac injection tests using multiple analysis methods. *SPE Prod. Oper.* **2009**, *24*, 396–406. [CrossRef]
27. Gu, H.; Elbel, J.; Nolte, K.; Cheng, A.D.; Abousleiman, Y. Formation permeability determination using impulse-fracture injection. In Proceedings of the SPE Production Operations Symposium, Oklahoma City, OK, USA, 21–23 May 1993.
28. Soliman, M.; Ansah, J. Methods and Systems for Using Wavelet Analysis in Subterranean Applications. U.S. Patent 6,978,211, 20 December 2005.
29. Craig, D.P.; Blasingame, T.A. Application of a new fracture-injection/falloff model accounting for propagating, dilated, and closing hydraulic fractures. In Proceedings of the SPE Gas Technology Symposium, The Woodlands, TX, USA, 1–3 April 2006.
30. Nolte, K.; Maniere, J.; Owens, K. After-closure analysis of fracture calibration tests. In Proceedings of the SPE Annual Technical Conference and Exhibition, San Antonio, TX, USA, 5–8 October 1997.
31. Marongiu-Porcu, M.; Ehlig-Economides, C.A.; Economides, M.J. Global model for fracture falloff analysis. In Proceedings of the North American Unconventional Gas Conference and Exhibition, The Woodlands, TX, USA, 14–16 June 2011.
32. Marongiu-Porcu, M.; Retnanto, A.; Economides, M.J.; Ehlig-Economides, C. Comprehensive fracture calibration test design. In Proceedings of the SPE Hydraulic Fracturing Technology Conference, The Woodlands, TX, USA, 4–6 February 2014.
33. Soliman, M.; Kabir, C. Testing unconventional formations. *J. Pet. Sci. Eng.* **2012**, *92*, 102–109. [CrossRef]
34. Cramer, D.; Nguyen, D. Diagnostic fracture injection testing tactics in unconventional reservoirs. In Proceedings of the SPE Hydraulic Fracturing Technology Conference, The Woodlands, TX, USA, 4–6 February 2013.
35. Padmakar, A. Geomechanics coupled reservoir flow simulation for diagnostic fracture injection test design and interpretation in shale reservoirs. In Proceedings of the SPE Annual Technical Conference and Exhibition, New Orleans, LA, USA, 30 September–2 October 2013.
36. Wallace, J.; Kabir, C.; Cipolla, C. Multiphysics investigation of diagnostic fracture injection tests in unconventional reservoirs. In Proceedings of the SPE Hydraulic Fracturing Technology Conference, The Woodlands, TX, USA, 4–6 February 2014.
37. Meng, C.; Wei, L.; Yuan, R.S.C. Coupled fluid flow and geomechanics modeling for DFIT analysis in unconventional gas development. In Proceedings of the International Petroleum Technology Conference, Kuala Lumpur, Malaysia, 10–12 December 2014.
38. Craig, D.P. New type curve analysis removes limitations of conventional after-closure analysis of DFIT data. In Proceedings of the SPE Unconventional Resources Conference, The Woodlands, TX, USA, 1–3 April 2014.
39. Sullivan, M.; Zanganeh, B.; Springer, A.; Clarkson, C. Post-fracture pressure decay: A novel (and free) stage-level assessment method. In Proceedings of the SPE/AAPG/SEG Unconventional Resources Technology Conference, Denver, CO, USA, 22–24 July 2019.
40. Hawkes, R.; Bachman, R.; Nicholson, K.; Cramer, D.; Chipperfield, S. Good Tests Cost Money, Bad Tests Cost More-A Critical Review of DFIT and Analysis Gone Wrong. In Proceedings of the SPE International Hydraulic Fracturing Technology Conference and Exhibition, Muscat, Oman, 16–18 October 2018.
41. McClure, M.W. Diagnostic fracture-injection tests with complex fracture networks. *Lead. Edge* **2014**, *33*, 546–552. [CrossRef]
42. McClure, M.W.; Jung, H.; Cramer, D.D.; Sharma, M.M. The fracture-compliance method for picking closure pressure from diagnostic fracture-injection tests. *SPE J.* **2016**, *21*, 1321–1339. [CrossRef]
43. Jung, H.; Sharma, M.M.; Cramer, D.D.; Oakes, S.; McClure, M.W. Re-examining interpretations of non-ideal behavior during diagnostic fracture injection tests. *J. Pet. Sci. Eng.* **2016**, *145*, 114–136. [CrossRef]
44. Wang, H.; Sharma, M.M. New Variable Compliance Method for Estimating In-Situ Stress and Leak-Off from DFIT Data. In Proceedings of the SPE Annual Technical Conference and Exhibition, San Antonio, TX, USA, 9–11 October 2017
45. Barree, R.D.; Barree, V.L.; Craig, D. Holistic fracture diagnostics. In Proceedings of the Rocky Mountain Oil & Gas Technology Symposium, Denver, CO, USA, 16–18 April 2007.
46. McClure, M.; Bammidi, V.; Cipolla, C.; Cramer, D.; Martin, L.; Savitski, A.A.; Sobernheim, D.; Voller, K. A collaborative study on DFIT interpretation: Integrating modeling, field data, and analytical techniques. In Proceedings of the Unconventional Resources Technology Conference, Denver, CO, USA, 22–24 July 2019; pp. 2020–2058.
47. Sneddon, I.N. The distribution of stress in the neighbourhood of a crack in an elastic solid. *Proc. R. Soc. Lond. Ser. A Math. Phys. Sci.* **1946**, *187*, 229–260.
48. Mcclure, M.; Fowler, G.; Picone, M. Best practices in DFIT interpretation: Comparative analysis of 62 DFITs from nine different shale plays. In Proceedings of the SPE International Hydraulic Fracturing Technology Conference & Exhibition, Muscat, Oman, 11–13 January 2022.
49. Rioul, O.; Vetterli, M. Wavelets and signal processing. *IEEE Signal Process. Mag.* **1991**, *8*, 14–38. [CrossRef]

50. Kaiser, G.; Hudgins, L.H. *A Friendly Guide to Wavelets*; Springer: Berlin/Heidelberg, Germany, 1994; Volume 300.
51. Addison, P.S. *The Illustrated Wavelet Transform Handbook: Introductory Theory and Applications in Science, Engineering, Medicine and Finance*; CRC Press: Boca Raton, FL, USA, 2017.
52. Guerrero, A.P.; Paredes, G.E. *Linear and Non-Linear Stability Analysis in Boiling Water Reactors: The Design of Real-Time Stability Monitors*; Woodhead Publishing: Sawston, UK, 2018.
53. Torrence, C.; Compo, G.P. A practical guide to wavelet analysis. *Bull. Am. Meteorol. Soc.* **1998**, *79*, 61–78. [CrossRef]

Disclaimer/Publisher's Note: The statements, opinions and data contained in all publications are solely those of the individual author(s) and contributor(s) and not of MDPI and/or the editor(s). MDPI and/or the editor(s) disclaim responsibility for any injury to people or property resulting from any ideas, methods, instructions or products referred to in the content.